

Digital Discovery

Accepted Manuscript

This article can be cited before page numbers have been issued, to do this please use: M. Q. Ha, D. Le, V. Nguyen, H. Kino, S. Curtarolo and H. Dam, *Digital Discovery*, 2025, DOI: 10.1039/D5DD00400D.



This is an Accepted Manuscript, which has been through the Royal Society of Chemistry peer review process and has been accepted for publication.

Accepted Manuscripts are published online shortly after acceptance, before technical editing, formatting and proof reading. Using this free service, authors can make their results available to the community, in citable form, before we publish the edited article. We will replace this Accepted Manuscript with the edited and formatted Advance Article as soon as it is available.

You can find more information about Accepted Manuscripts in the [Information for Authors](#).

Please note that technical editing may introduce minor changes to the text and/or graphics, which may alter content. The journal's standard [Terms & Conditions](#) and the [Ethical guidelines](#) still apply. In no event shall the Royal Society of Chemistry be held responsible for any errors or omissions in this Accepted Manuscript or any consequences arising from the use of any information it contains.

1 Beyond Interpolation: Integration of Data and AI-Extracted Knowledge

2 for High-Entropy Alloy Discovery

3 Minh-Quyet Ha,¹ Dinh-Khiet Le,¹ Viet-Cuong Nguyen,² Hiori Kino,³ Stefano Curtarolo,^{4,5} and Hieu-Chi
4 Dam^{1,6,a)}

5 ¹⁾Japan Advanced Institute of Science and Technology, 1-1 Asahidai, Nomi, Ishikawa 923-1292,
6 Japan

7 ²⁾HPC SYSTEMS Inc., 3-9-15 Kaigan, Minato, Tokyo 108-0022, Japan

8 ³⁾Research Center for Materials Informatics, Department of Advanced Data Science,
9 The Institute of Statistical Mathematics, 10-3 Midori-cho, Tachikawa, Tokyo 190-8562,
10 Japan

11 ⁴⁾Department of Mechanical Engineering and Materials Science, Duke University, Durham, NC 27708,
12 USA

13 ⁵⁾Center for Extreme Materials, Duke University, Durham, NC 27708, USA

14 ⁶⁾International Center for Synchrotron Radiation Innovation Smart (SRIS), Tohoku University, 2-1-1 Katahira,
15 Aoba-ku, Sendai 980-8577, Japan

16 (Dated: 14 December 2025)

17 Discovering novel high-entropy alloys (HEAs) with desirable properties is challenged by the vast compositional
18 space and the complexity of phase formation mechanisms. Several inductive screening methods that excel
19 at interpolation have been developed; however, they struggle with extrapolating to novel alloy systems.
20 This study introduces a framework that addresses the extrapolation limitation by systematically integrating
21 knowledge extracted from material datasets with expert knowledge derived from scientific literature using large
22 language models (LLMs). Central to our framework is the elemental substitution principle, which identifies
23 chemically similar elements that can be interchanged while preserving desired properties. To model and
24 combine evidence from these multiple sources of knowledge, we employ the Dempster–Shafer theory, which
25 provides a mathematical foundation for reasoning under uncertainty. Our framework consistently outperforms
26 conventional phase selection models that rely on single-source knowledge across all experiments, showing
27 notable advantages in predicting phase stability for compositions containing elements absent from training
28 data. Importantly, the framework effectively complements the strengths of the existing methods. Moreover,
29 it provides interpretable reasoning that elucidates element substitutability patterns critical to alloy stability
30 in HEA formation. These results highlight the framework's potential for knowledge integration, offering an
31 efficient approach to exploring the vast compositional space of HEAs with enhanced generalizability and
32 interpretability.

33 I. INTRODUCTION

34 High-entropy alloys (HEAs), also known as multi-
35 principal element alloys (MPEAs), have garnered sig-
36 nificant attention owing to their exceptional mech-
37 ical properties, thermal stability, and corrosion resis-
38 tance^{1–3}. Typically consisting of five or more princi-
39 pal elements in near-equatomic ratios, these alloys uti-
40 lize high-configurational entropy to stabilize single-phase
41 solid solutions^{4–6}. However, identifying stable composi-
42 tions remains a significant challenge due to the vast com-
43 positional space and the complex interplay of factors such
44 as mixing entropy, enthalpy, atomic size differences, and
45 electronic structure. These challenges, including explor-
46 ing expansive design spaces, handling sparse data, and
47 managing uncertainty, represent broader issues in com-
48 binatorial materials research, where efficient navigation
49 strategies of compositional possibilities are essential.

50 A useful framework for understanding this challenge is
51 a decision-making model in which researchers must bal-

52 ance *exploitation* and *exploration*^{7,8}, as illustrated in Fig-
53 ure 1. Exploitation focuses on well-characterized regions
54 of the design space, having sufficient data for reliable
55 property predictions. This approach supports steady,
56 incremental improvements to existing alloys. In these
57 data-rich regions, uncertainty is primarily *aleatoric*, aris-
58 ing from irreducible variability within the system. Con-
59 versely, exploration targets novel regions where data is
60 insufficient for reliable property predictions. These re-
61 gions introduce higher *epistemic* uncertainty that can be
62 decreased as we collect more data through systematic ex-
63 perimentation. Although exploration bears greater risk,
64 it offers the exciting potential to uncover groundbreaking
65 and fundamentally new alloys with exceptional prop-
66 erties. Achieving an optimal balance between these two
67 strategies is crucial for advancing HEA development.

68 Data-driven methods have emerged as transformative
69 tools for guiding these exploitation-exploration decisions,
70 enabling the processing of large datasets and streamlin-
71 ing the search for promising HEAs^{9–13}. High-throughput
72 approaches, such as CALPHAD^{3,14,15}, AFLOW^{16–18},
73 and Hamiltonian models^{19,20}, alongside machine learning
74 (ML)²¹, have significantly reduced the time and cost as-
75 sociated with evaluating candidate compositions. While

^{a)}Electronic mail: dam@jaist.ac.jp



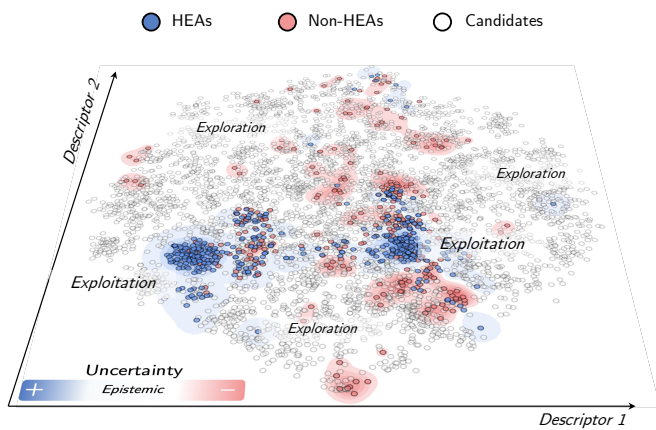


FIG. 1. Illustration of decision-making scenarios in high-entropy alloy (HEA) discovery. Colored regions represent well-established areas of the HEA compositional space, characterized by sufficient data suitable for effective exploitation. In contrast, white regions depict unexplored areas with sparse or no existing data, highlighting opportunities for risky yet potentially transformative exploration that could lead to discovering groundbreaking alloys with fundamentally new and exceptional properties. HEAs and Non-HEAs denote alloys that respectively form or do not form a stable high-entropy phase.

1 conventional ML models excel at *interpolation*, accu-
2 rately predicting outcomes for compositions similar to
3 those in the training sets (supporting exploitation), they
4 struggle with *extrapolation* to novel systems, limiting ex-
5 ploration capability²². Although careful feature engi-
6 neering can partially address extrapolation challenges²³,
7 designing features that generalize across vast composi-
8 tional spaces remains practically difficult^{22,24}. This *in-*
9 *terpolation-extrapolation* dichotomy needs to be over-
10 come as HEA discovery obviously requires venturing into
11 uncharted territory.

12 A critical aspect of managing exploration-exploitation
13 balance is uncertainty quantification, which falls into two
14 categories. Epistemic uncertainty arises from incomplete
15 or sparse data and is reducible through targeted informa-
16 tion gathering, while aleatoric uncertainty corresponds to
17 intrinsic variability within the system and is irreducible
18 regardless of data volume²⁵. Traditional methods, such
19 as Bayesian neural networks, Gaussian processes, and
20 Monte Carlo dropout, are commonly employed to quan-
21 tify these uncertainties^{26,27}. However, they often falter
22 in early-stage materials discovery, where data is sparse
23 or conflicting²⁸⁻³⁰.

24 An alternative framework, the Dempster-Shafer the-
25 ory³¹⁻³³, also known as evidence theory, offers a more
26 flexible means of representing uncertainty. Unlike
27 Bayesian methods, which assign probabilities to indi-
28 vidual elements within a set of possibilities (denoted as
29 Ω), evidence theory assigns non-negative weights (sum-
30 ming to one) to subsets of Ω . This enables the ex-
31 plicit representation of ignorance rather than requiring

32 an assumption about a prior probability distribution²⁵,
33 allowing for nuanced characterization of both epistemic
34 and aleatoric uncertainties. Thus, this framework can
35 guide researchers to specific regions of the compositional
36 space for either efficient exploitation or effective explo-
37 ration^{22,34,35}.

38 However, collecting additional data to reduce epis-
39 temic uncertainty is often impractical due to high costs
40 and experimental constraints. Expert knowledge offers a
41 valuable alternative for mitigating this uncertainty. Do-
42 main specialists bring insights accumulated across multi-
43 ple studies and contexts, providing heuristics that extend
44 beyond any single dataset³⁶⁻³⁸. Physics-informed neural
45 networks (PINNs) exemplify one approach to incorpo-
46 rating domain knowledge by embedding a priori physical
47 laws, enabling inference of governing equations from lim-
48 ited observations when those laws are explicit and well-
49 defined³⁹. Yet their performance degrades when the un-
50 derlying physics is only partially understood or key con-
51 straints remain unknown. More broadly, expert knowl-
52 edge often resides in unstructured forms, such as labora-
53 tory notebooks, informal rules of thumb, or tacit experi-
54 ence, making its integration with structured, data-driven
55 models a significant challenge.

56 To bridge this gap, this study introduces a framework
57 that integrates knowledge from material datasets with
58 expert domain knowledge accessed through AI systems—
59 in this implementation, large language models (LLMs)
60 extracting insights from scientific literature—while ac-
61 counting for inherent uncertainties in each source. This
62 uncertainty-aware integration enables systematic predic-
63 tions beyond the interpolative boundaries of conventional
64 data-driven methods. Central to our methodology is the
65 *elemental substitution* principle^{40,41}, a well-established
66 concept in alloy design wherein chemically similar ele-
67 ments can be interchanged while preserving target prop-
68 erties. We treat observed alloy pairs as evidence for
69 substitutability patterns, then consolidate this empirical
70 data with AI-derived insights obtained through state-of-
71 the-art LLMs, including GPT-4o, GPT-4.5, Claude Opus
72 4, and Grok3. These LLMs leverage documented knowl-
73 edge from related scientific domains through *knowledge*
74 *integration* to assess elemental substitutability beyond
75 the training dataset, not by generating information be-
76 yond their training corpus. Through Dempster-Shafer
77 theory, the framework systematically models and com-
78 bines these diverse evidence sources while quantifying
79 both epistemic and aleatoric uncertainties. By providing
80 accurate predictions in well-characterized regions along-
81 side uncertainty-aware guidance for data-sparse spaces,
82 this framework demonstrates—using HEAs as a proof
83 of concept—the viability of materials discovery through
84 uncertainty-aware AI integration.

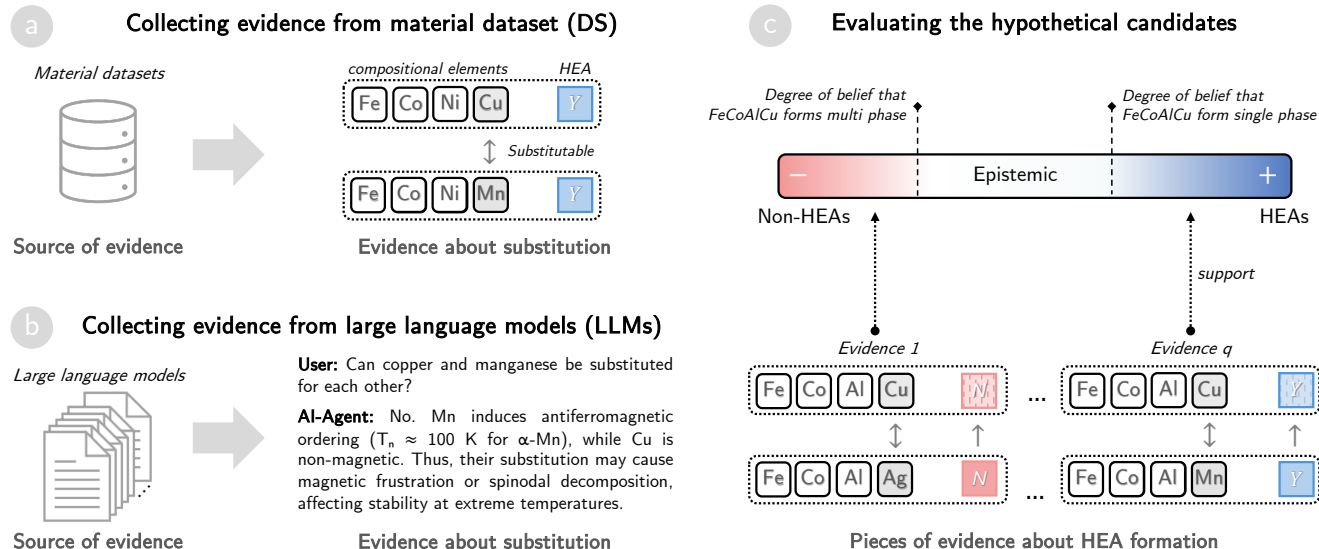


FIG. 2. Hybrid framework integrating Data and AI-extracted Knowledge for high-entropy alloy (HEA) discovery. (a–b) Schematic depicting the collection of substitutability evidence from a single material dataset (DS) and large language models (LLMs). (c) Schematic illustrating the assessment of hypothetical candidate properties using aggregated evidence derived from substitution-based methods.

II. METHODOLOGY

Each alloy A in the dataset \mathcal{D} is represented by its constituent elements. The property of interest y_A , for any alloy A , can be either *HEA* or $\overline{\text{HEA}}$. Here, *HEA* denotes alloys that form a stable high-entropy phase (single-phase solid solution), while $\overline{\text{HEA}}$ (or Non-*HEA*) denotes alloys that do not form a stable high-entropy phase (multi-phase structures). To determine elemental substitutability, we assess the similarity between different element combinations by adapting *evidence theory*, which models and aggregates diverse pieces of evidence obtained from \mathcal{D} . Similarities between objects can manifest in various forms⁴²; e.g., pairwise ratings, object sorting, communal associations, substitutability, and correlation. In this study, we specifically focus on the *solid-solution formability* of element combinations and quantify their similarities based on elemental substitutability.

Our approach is intuitively illustrated using the example of element substitutability between Mn and Cu in Figure 2. Suppose we observe from materials datasets that two alloys, FeCoNiCu and FeCoNiMn, both form HEAs. This provides evidence that Cu can substitute for Mn in this context. Meanwhile, consulting domain knowledge through LLMs might reveal that metallurgists consider Cu-Mn pairs as non-substitutable, contributing additional conflicting evidence. Our proposed framework models and combines these independent pieces of evidence using evidence theory, potentially resulting in stronger belief in their substitutability than either source alone would provide. When predicting whether a new alloy, such as FeCoAlCu, forms an HEA, the framework can leverage existing data about FeCoAlMn and the es-

tablished Cu-Mn substitutability to make informed predictions.

A. Transforming Materials Data to Substitutability Evidence

Consider two alloys, A_i and A_j in \mathcal{D} , that share at least one common element. This non-disjoint pair of alloys provides evidence regarding the substitutability between the element combinations:

$$C_t = A_i \setminus (A_i \cap A_j) \quad \text{and} \quad C_v = A_j \setminus (A_i \cap A_j).$$

The intersection $A_i \cap A_j$ serves as the *context* for measuring similarity. If y_{A_i} and y_{A_j} agree (i.e., both are classified as *HEA* or both as $\overline{\text{HEA}}$), we infer that C_t and C_v are substitutable; otherwise, they are non-substitutable, as shown in Figure 2a.

The symmetric substitutability assumption ($C_t \rightarrow C_v$ and $C_v \rightarrow C_t$ are the same) used in this work represents a context-averaged approximation. While empirically validated for near-equiatomic HEAs, this assumption may limit accuracy for systems with strong directional substitution preferences. However, this symmetric treatment is justified in this study by two factors: first, the limited training data in our data-sparse scenarios makes learning separate directional patterns statistically infeasible; second, for near-equiatomic multi-principal element HEAs characterized by disordered random solid solutions, elements occupy statistically similar local environments, rendering symmetric substitution a physically reasonable first-order approximation.

Evidence for similarity is captured by defining a *frame of discernment*³² $\Omega_{\text{sim}} = \{\text{similar}, \text{dissimilar}\}$, encom-

1 passing all possible outcomes. The evidence from A_i and
 2 A_j is then represented by a *mass function* (or *basic prob-*
 3 *ability assignment*) $m_{A_i, A_j}^{C_t, C_v}$. This mass function assigns
 4 non-zero probability to the non-empty subsets of Ω_{sim} ,
 5 as:

$$m_{A_i, A_j}^{C_t, C_v}(\{\text{similar}\}) = \begin{cases} \alpha, & \text{if } y_{A_i} = y_{A_j}, \\ 0, & \text{otherwise,} \end{cases} \quad (1)$$

$$m_{A_i, A_j}^{C_t, C_v}(\{\text{dissimilar}\}) = \begin{cases} \alpha, & \text{if } y_{A_i} \neq y_{A_j}, \\ 0, & \text{otherwise,} \end{cases} \quad (2)$$

$$m_{A_i, A_j}^{C_t, C_v}(\Omega_{sim}) = 1 - \alpha. \quad (3)$$

6 Here, the parameter $0 < \alpha < 1$ is determined through
 7 an exhaustive search for optimal cross-validation per-
 8 formance, as shown in Supplementary Section 1. Intu-
 9 itively, $m_{A_i, A_j}^{C_t, C_v}(\{\text{similar}\})$ and $m_{A_i, A_j}^{C_t, C_v}(\{\text{dissimilar}\})$ rep-
 10 resent the extent to which alloys A_i and A_j support sub-
 11 stitutability or non-substitutability of C_t and C_v . Fur-
 12 ther, $m_{A_i, A_j}^{C_t, C_v}(\Omega_{sim})$ encodes epistemic uncertainty (i.e.,
 13 lack of definitive information). The probabilities assigned
 14 to these three subsets of Ω_{sim} must sum to 1.

15 Assuming that we collect q pieces of evidence from \mathcal{D}
 16 to compare C_t and C_v , each piece of evidence corresponds
 17 to a pair of alloys that generates a mass function $m_i^{C_t, C_v}$.
 18 These q mass functions are combined via *Dempster's rule*
 19 of combination³¹ to obtain a joint mass function $m_{\mathcal{D}}^{C_t, C_v}$:

$$m_{\mathcal{D}}^{C_t, C_v}(\omega) = \left(m_1^{C_t, C_v} \oplus m_2^{C_t, C_v} \oplus \dots \oplus m_q^{C_t, C_v} \right)(\omega), \quad (4)$$

20 where $\omega \subseteq \Omega_{sim}$, $\omega \neq \emptyset$ and \oplus denotes the Dempster's
 21 rule of combinations, as described in Supplementary Sec-
 22 tion 2. When no relevant evidence is available, $m_{\mathcal{D}}^{C_t, C_v}$
 23 is initialized with a mass of 1 on $\{\text{similar, dissimilar}\}$,
 24 indicating total uncertainty.

25 B. Transforming Domain Knowledge to Substitutability 26 Evidence

27 In addition to evidence collected from material
 28 datasets (DS), we focus on evidence derived from do-
 29 main knowledge, utilizing LLMs to extract insights from
 30 a vast corpus of scientific literature. Specifically, we use
 31 a set of state-of-the-art LLMs including GPT-4o, GPT-
 32 4.5, Claude Opus 4, and Grok3 to assess element sub-
 33 stitutability based on expert perspectives within a given
 34 domain, as illustrated in Figure 2b. The proposed model
 35 evaluates the substitutability of element pairs from the
 36 perspective of a domain expert, ensuring that the anal-
 37 ysis aligns with established scientific reasoning. To en-
 38 hance result reliability, we implement a two-step prompt-
 39 ing procedure:

40 • **Question 1:** Do you possess sufficient knowledge
 41 or data to evaluate the substitutability of elements
 42 C_t and C_v within the context of */domain knowl-*
 43 *edge/*?

44 • **Question 2:** If the answer to the first question is
 45 Yes, the LLM further rates element substitutability
 46 as High, Medium, or Low, based on insights distilled
 47 from relevant scientific literature in the given do-
 48 main.

49 Detailed prompts used for each LLM are provided in
 50 Supplementary File 1. This approach is based on the as-
 51 sumption that, when given clear and structured prompts,
 52 these LLMs can simulate expert reasoning across multi-
 53 ple scientific domains. This capability stems from their
 54 extensive training on scientific literature, which enables
 55 them to provide contextually relevant, domain-specific
 56 feedback tailored to the challenges of HEA discovery.

57 Elemental substitutability is not universal and is
 58 property-specific, strongly associated with functionality
 59 and applications. For example, substitution targeting the
 60 structural stability differs from substitution targeting the
 61 magnetic, optical, or mechanical properties. Recogniz-
 62 ing this property-specific nature, our framework requires
 63 careful domain selection tailored to the target property
 64 to ensure accurate predictions. To facilitate the extrac-
 65 tion of domain knowledge, we focus on five key scientific
 66 domains, including *corrosion science*, *materials mechan-*
 67 *ics*, *metallurgy*, *solid-state physics*, and *materials science*.
 68 These domains are selected due to their critical roles in
 69 understanding and optimizing HEAs, specifically tailored
 70 for phase stability prediction⁵. Each domain contributes
 71 essential insights into different aspects of alloy design.

72 • **Corrosion science:** This domain examines chem-
 73 ical degradation mechanisms and protective strate-
 74 gies, essential for ensuring long-term durability.

75 • **Materials mechanics:** This domain investigates
 76 mechanical properties such as strength, ductility,
 77 and toughness, crucial for structural performance.

78 • **Metallurgy:** This domain analyzes phase forma-
 79 tion, phase diagrams, and microstructure control,
 80 offering insights into alloy stability and processing
 81 methods.

82 • **Solid-state physics:** This domain explores
 83 atomic-scale interactions, electronic structure, and
 84 thermal behavior, all of which influence phase sta-
 85 bility and material performance.

86 • **Materials science:** This domain serves as an inte-
 87 grative field that synthesizes perspectives from the
 88 other domains, emphasizing the relationships be-
 89 tween composition, structure, properties, and per-
 90 formance to optimize alloy design strategies.

91 The evidence collected from the LLM for each do-
 92 main is categorized into one of four outcomes: High,



TABLE I. Possible outcomes generated by an LLM for each domain-specific criterion, along with the corresponding mass functions $m_{\text{LLMs}}^{C_t, C_v}(\{\text{similar}\})$, $m_{\text{LLMs}}^{C_t, C_v}(\{\text{dissimilar}\})$, and $m_{\text{LLMs}}^{C_t, C_v}(\{\text{similar, dissimilar}\})$. Here, $0 < \beta < 1$ indicates our confidence in LLM's response, with determination details provided in Supplementary Section 1.

Q1	Q2	$m_{\text{LLMs}}^{C_t, C_v}(\{\text{similar}\})$	$m_{\text{LLMs}}^{C_t, C_v}(\{\text{dissimilar}\})$	$m_{\text{LLMs}}^{C_t, C_v}(\Omega_{\text{sim}})$	Interpretation
No	—	0	0	1	LLM does not provide sufficient domain knowledge
Yes	High	β	0	$1 - \beta$	C_t and C_v are considered <i>highly</i> substitutable
Yes	Medium	$\beta/2$	$\beta/2$	$1 - \beta$	C_t and C_v are considered <i>moderately</i> substitutable
Yes	Low	0	β	$1 - \beta$	C_t and C_v are considered <i>poorly</i> substitutable

1 Medium, Low, or No Knowledge. Further, these outcomes
2 are mapped to a corresponding mass function denoted
3 as $m_{\text{LLMs}}^{C_t, C_v}$, as shown in Table I. If the LLM indicates No
4 Knowledge, then the entire mass is assigned to the set
5 $\{\text{similar, dissimilar}\}$, reflecting complete epistemic uncer-
6 tainty. Conversely, if the LLM provides a specific substi-
7 tutability rating (High, Medium, and Low), then a portion
8 of the mass is allocated to either $\{\text{similar}\}$ or $\{\text{dissimilar}\}$,
9 while the remaining mass is assigned to Ω_{sim} to account
10 for residual uncertainty in the prediction.

11 Notably, all LLMs (GPT-4o, GPT-4.5, Claude Opus
12 4, and Grok3) are used as pre-trained models *out-of-*
13 *the-box* without any fine-tuning, retraining, or in-context
14 literature provision. These models are queried directly
15 through their respective API interfaces using the two-
16 step prompting procedure described above and detailed
17 in Supplementary File 1. The LLMs leverage knowledge
18 from scientific literature encountered during their origi-
19 nal pre-training by the respective model developers; we
20 do not modify these models in any way. Each LLM pro-
21 vides independent assessments that are later combined
22 using Dempster-Shafer theory (Section II.C).

23 C. Combining Evidence from Multiple Sources

24 In this study, a *source* S refers to an independent
25 knowledge provider that generates evidence about ele-
26 mental substitutability. Our multi-source framework in-
27 tegrates two kinds of independent sources:

- 28 • **DS-source:** A material dataset \mathcal{D} provides em-
29 pirical evidence by analyzing alloy pairs that differ
30 by element substitution (Section II A). This dataset
31 contains factual observations about the target do-
32 main (e.g., which alloy compositions form HEAs).
- 33 • **LLM sources:** We query 4 state-of-the-art LLMs
34 (GPT-4o, GPT-4.5, Claude Opus 4, Grok3) across
35 5 scientific domains (corrosion science, materials
36 mechanics, metallurgy, solid-state physics, materi-
37 als science), creating $4 \times 5 = 20$ independent knowl-
38 edge sources (Section II B). Each combination of an
39 LLM and a domain provides documented scientific
40 knowledge from related or similar domains to the
41 target domain.

42 To integrate substitutability evidence collected from
43 multiple sources, Dempster's rule of combination with a

44 *reliability-aware discounting* step is used^{32,43}. Recogniz-
45 ing that substitutability is property-specific and differ-
46 ent sources capture different aspects of elemental substi-
47 tutability, our framework implements an adaptive mech-
48 anism that evaluates each source's relevance to the target
49 property. This reliability-aware discounting automati-
50 cally assigns higher weights to sources that align well with
51 the specific property being predicted while suppressing
52 sources that capture irrelevant substitutability criteria,
53 thereby preventing inappropriate knowledge integration.

54 For each source S , we compute a dataset-specific dis-
55 count factor as:

$$\gamma_S = \text{disc}(m_S^{C_t, C_v}, \mathcal{D}) \in [0, 1], \quad (5)$$

56 where $\text{disc}(\cdot)$ quantifies how well the substitutability ev-
57 idence collected from source S generalizes to the alloy
58 properties in \mathcal{D} . The reliability of each source is assessed
59 using the macro-averaged F1 score with 10-fold cross-
60 validation. For instance, if a source S has historically
61 demonstrated accurate predictions on alloys similar to
62 those in \mathcal{D} , we assign γ_S a value closer to 1. Conversely,
63 if S performs poorly or unpredictably for alloys in \mathcal{D} , γ_S
64 is reduced accordingly.

65 The original mass function $m_S^{C_t, C_v}$ for source S is then
66 modified by incorporating the discount factor γ_S , leading
67 to an adjusted function $\gamma_S m_S^{C_t, C_v}$:

$$\begin{aligned} \gamma_S m_S^{C_t, C_v}(\{\text{similar}\}) &= \gamma_S \times m_S^{C_t, C_v}(\{\text{similar}\}), \\ \gamma_S m_S^{C_t, C_v}(\{\text{dissimilar}\}) &= \gamma_S \times m_S^{C_t, C_v}(\{\text{dissimilar}\}), \\ \gamma_S m_S^{C_t, C_v}(\Omega_{\text{sim}}) &= 1 - \gamma_S + \gamma_S \times m_S^{C_t, C_v}(\Omega_{\text{sim}}). \end{aligned} \quad (6)$$

68 This redistribution shifts mass from definitive conclu-
69 sions $\{\text{similar}\}$ and $\{\text{dissimilar}\}$ to the ambiguous set
70 $\{\text{similar, dissimilar}\}$, thereby encoding epistemic uncer-
71 tainty for less reliable sources. Therefore, when all mass
72 functions are subsequently merged using Dempster's rule,
73 less credible sources exert a weaker influence on the final
74 decision.

75 Assuming p sources $\{S_1, S_2, \dots, S_p\}$, the substitutabil-
76 ity evidence gathered from them is aggregated using
77 Dempster's rule of combination:

$$m^{C_t, C_v}(\omega) = \left(\gamma_{S_1} m_{S_1}^{C_t, C_v} \oplus \gamma_{S_2} m_{S_2}^{C_t, C_v} \oplus \dots \oplus \gamma_{S_p} m_{S_p}^{C_t, C_v} \right)(\omega), \quad (7)$$

1 where ω denotes non-empty subsets of Ω_{sim} . The rule it-
 2 eratively integrates evidence while normalizing conflicts
 3 (such as empty-set intersections arising from contradic-
 4 tory sources). This approach preserves diverse insights,
 5 from data-driven correlations to LLM-derived domain
 6 knowledge, while mitigating the influence of unreliable
 7 sources. Critically, when evidence about substitutability
 8 is insufficient or conflicting, Dempster's rule of combina-
 9 tion assigns high mass to $m^{C_t, C_v}(\Omega_{sim})$, explicitly signal-
 10 ing uncertainty rather than forcing confident predictions.
 11 This naturally prevents overfitting in data-sparse scenar-
 12 ios common in materials discovery.

13 Similar analyses are conducted for all pairs of element
 14 combinations, resulting in a symmetric matrix M , where
 15 $(M[t, v] = M[v, t] = m^{C_t, C_v}(\{\text{similar}\}))$.

16 D. Evaluating Hypothetical Candidates by Analogy-Based 17 Inference

18 To predict whether a *new* alloy A_{new} is likely to form
 19 an HEA, we employ a substitution-based inference ap-
 20 proach utilizing the similarity matrix M . The process
 21 begins with a known alloy A_k , labeled y_{A_k} , and iden-
 22 tifies the subset $C_t \subset A_k$ that, when replaced by C_v ,
 23 generates A_{new} (Figure 2 c). If C_t and C_v are deemed
 24 substitutable, then $y_{A_{new}}$ is more likely to match y_{A_k} ;
 25 conversely, if they are dissimilar, $y_{A_{new}}$ may differ.

26 We formalize this inference using a frame of discern-
 27 ment³² $\Omega_{HEA} = \{\text{HEA}, \overline{\text{HEA}}\}$ and define a mass function
 28 $m_{A_k, C_t \leftarrow C_v}^{A_{new}}$ to model the evidence collected from A_k and
 29 the substitution of C_t , for C_v , denoted as $C_t \leftarrow C_v$. This
 30 mass function distributes belief among $\{\text{HEA}\}$, $\{\overline{\text{HEA}}\}$,
 31 or $\{\text{HEA}, \overline{\text{HEA}}\}$ according to the similarity $M[t, v]$ and
 32 the label of A_k as:

$$m_{A_k, C_t \leftarrow C_v}^{A_{new}}(\{\text{HEA}\}) = \begin{cases} M[t, v], & \text{if } y_{A_k} = \text{HEA}, \\ 0, & \text{otherwise,} \end{cases} \quad (8)$$

$$m_{A_k, C_t \leftarrow C_v}^{A_{new}}(\{\overline{\text{HEA}}\}) = \begin{cases} M[t, v], & \text{if } y_{A_k} = \overline{\text{HEA}}, \\ 0, & \text{otherwise,} \end{cases} \quad (9)$$

$$m_{A_k, C_t \leftarrow C_v}^{A_{new}}(\Omega_{HEA}) = 1 - M[t, v]. \quad (10)$$

33 Here, the probability mass assigned to $\{\text{HEA}\}$ and
 34 $\{\overline{\text{HEA}}\}$ reflects the confidence levels with which A_k and
 35 the substitution of C_v for C_t support the probabilities
 36 that A_{new} is or is not an HEA, respectively. The mass
 37 assigned to subset $\{\text{HEA}, \overline{\text{HEA}}\}$ represents epistemic
 38 uncertainty, signifying cases where the available evidence
 39 does not provide definitive information regarding the
 40 properties of A_{new} . The total probability mass assigned
 41 to all three non-empty subsets of Ω_{HEA} is constrained to
 42 sum to 1, ensuring a consistent probabilistic framework.
 43 An illustrative example employing the Dempster-Shafer

44 theory for the evaluation of hypothetical candidates is
 45 provided in Supplementary Section 3.

46 We assume that multiple pieces of evidence can be
 47 collected, each derived from a distinct pair of host al-
 48 loy A_{host} and substitution pair $C_t \leftarrow C_v$, for a new
 49 alloy candidate A_{new} . These individual pieces of evi-
 50 dence are systematically combined using Dempster's rule
 51 of combination to generate a final mass function $m^{A_{new}}$.
 52 This function integrates all available analogies, resolving
 53 potential inconsistencies and contradictions among the
 54 sources. The resulting combined evidence offers a coher-
 55 ent assessment, aiding in informed decision-making re-
 56 garding whether further resource-intensive experiments
 57 are necessary to validate the HEA formation ability of
 58 A_{new} .

59 III. EXPERIMENTAL SETTING

60 In this section, we present the design of experiments,
 61 which assess both the *predictive capability* and *inter-
 62 pretability* of our proposed method. Additionally, we
 63 provide comparisons against alternative approaches, in-
 64 cluding single-source evidential methods and other data-
 65 driven classifiers.

66 A. Datasets

67 Experiments are conducted considering four compu-
 68 tational datasets of quaternary alloys, one experimen-
 69 tal dataset of quaternary alloys, and one experimental
 70 dataset of quinary high-entropy borides (HEB), summa-
 71 rized in Table II. HEBs are single-phase ceramics con-
 72 taining multiple transition metal cations randomly dis-
 73 tributed on the metal sublattice of a boride structure, of-
 74 fering unique combinations of metallic and ceramic prop-
 75 erties⁴⁴. Despite different bonding mechanisms, HEBs
 76 exhibit similarly high elemental selectivity as HEAs—
 77 boron's restrictive bonding requirements create stringent
 78 constraints on metal selection, analogous to the selec-
 79 tive substitutability patterns in metallic HEAs, making
 80 them suitable for testing our framework's core princi-
 81 ple of managing uncertainty in highly selective multi-
 82 component systems.

83 • $\mathcal{D}_{0.9T_m}$ and \mathcal{D}_{1350K} : These computational datasets
 84 include *all possible quaternary* alloys generated
 85 from a set of 26 elements: Fe, Co, Ir, Cu, Ni, Pt,
 86 Pd, Rh, Au, Ag, Ru, Os, Si, As, Al, Re, Mn, Ta,
 87 Ti, W, Mo, Cr, V, Hf, Nb, and Zr. The stabili-
 88 ty of these alloys is predicted using methods pro-
 89 posed by Chen *et al.*⁴⁵ at two different tempera-
 90 tures: $0.9T_m$ (approximately 90% of the melting
 91 temperature T_m of the alloy) and 1350 (K). These
 92 predictions are obtained via a high-throughput
 93 computational workflow, which employs a regular-
 94 solution model^{46,47} using binary interaction param-



TABLE II. Summary of alloy datasets used in evaluation experiments. No. alloys: Total number of alloys present in each dataset. No. positive label: Number of alloys classified as forming HEA phases in datasets $\mathcal{D}_{0.9T_m}$ and \mathcal{D}_{1350K} , the number of alloys exhibiting non-zero magnetization in \mathcal{D}_{Mag} , and the number of alloys with a non-zero Curie temperature in \mathcal{D}_{T_C} . The percentage values in parentheses represent the proportion of positive labels within each dataset.

Dataset	No. alloys	Physical properties	Positive label	No. positive label
$\mathcal{D}_{0.9T_m}$	14,950 quaternary alloys	Stability	HEA	4,218 (28%)
\mathcal{D}_{1350K}	14,950 quaternary alloys	Stability	HEA	1,402 (9%)
\mathcal{D}_{Mag}	5,968 quaternary alloys	Magnetization (T)	Magnetic	2,428 (41%)
\mathcal{D}_{T_C}	5,968 quaternary alloys	Curie temperature (K)	Non-zero Curie Temperature	2,355 (39%)
\mathcal{D}_{HEA}^{exp}	55 quaternary alloys	Stability	HEA	40 (73%)
\mathcal{D}_{HEB}^{exp}	19 quinary alloys-borides	Stability	HEB	15 (79%)

eters derived from *ab initio* density functional theory (DFT) to compute and compare Gibbs free energies of solid solutions against competing intermetallic phases^{16–18}.

- \mathcal{D}_{Mag} and \mathcal{D}_{T_C} : These computational datasets comprise 5,968 quaternary high-entropy alloys (HEAs)³⁵, each formed by selecting four elements from a set of 21 transition metals: Fe, Co, Ir, Cu, Ni, Pt, Pd, Rh, Au, Ag, Ru, Os, Tc, Re, Mn, Ta, W, Mo, Cr, V, and Nb. Their magnetizations (\mathcal{D}_{Mag}) and Curie temperatures (\mathcal{D}_{T_C}) in the body-centered cubic (BCC) phase are computed using the Korringa–Kohn–Rostoker coherent approximation method⁴⁸. These datasets are derived from an original pool of 147,630 equiatomic quaternary HEAs.
- \mathcal{D}_{HEA}^{exp} : The experimental dataset includes 55 experimentally verified quaternary HEAs from peer-reviewed publications^{45,49,50}. The dataset includes both HEA (40 alloys) and non-HEA (15 alloys) compositions, providing balanced representation for validation.
- \mathcal{D}_{HEB}^{exp} : The experimental dataset includes 19 experimentally verified quinary HEBs from peer-reviewed publications⁴⁴. The dataset includes 15 quinary systems forming HEB.

B. Design of experiments

We begin by verifying the reliability of the elemental substitutability knowledge queried from large language models (LLMs). Specifically, we compare the LLM-derived substitutability knowledge with the well-established Hume–Rothery criteria for elemental substitution.

With that reliability confirmed, we turn to predictive capability. Two experiments on four computational datasets serve as the framework’s proving ground to evaluate predictive capability of our proposed framework: (1) Cross-validation on quaternary alloys, assessing performance with randomly partitioned training sets (1%-30%

of data) to determine how effectively LLM-derived knowledge aligns with material-specific relationships across different data availability scenarios, with particular focus on data-limited conditions; and (2) Extrapolation on quaternary alloys, simulating real discovery scenarios by excluding alloys containing a specific element from training and evaluating performance on compositions that incorporate this previously unseen element. These computational datasets, free from experimental bias and large enough for robust statistics, provide the controlled environment needed for *framework development*.

To benchmark our multi-source method, we compare its predictive performance against two baseline approaches.

- **Single-source methods:** These methods rely exclusively on one source of evidence, either a material dataset or domain knowledge derived from only one LLM from the set of state-of-the-art models under investigation.
- **Traditional classification method:** We employ logistic regression (LR)⁵¹.

Hyper-parameters of these methods are tuned via systematic grid search, as detailed in Supplementary Section 1. Hereinafter, we define models employing the evidential method (based on the Dempster–Shafer theory) as follows: models trained solely on material datasets are termed DS-source models; those leveraging evidence from LLMs are termed LLM-source models; and those integrating both sources are termed multi-source models. Notably, the LLM-source models are obtained by combining 20 independent sources—each of the 4 LLMs (GPT-4o, GPT-4.5, Claude Opus 4, Grok3) queried across 5 scientific domains—through Dempster–Shafer theory (Section II C). The multi-source model further integrates this combined LLM-source with the DS-source using the same framework. Models utilizing logistic regression and support vector machines are referred to as LR-based model.

To assess the real-world applicability of our framework, we next validate its predictive performance on experimentally verified alloys. This validation examines whether the proposed framework can accurately predict phase stability for experimentally synthesized alloys. Our framework integrates LLM-derived knowledge with



TABLE III. Confusion matrix comparing LLM consensus predictions with Hume–Rothery rules for 351 element pairs considered in this study.

		Hume–Rothery rules		Total
		Substitutable	Non-substitutable	
LLMs	Substitutable	33 pairs (<i>True positive</i>)	45 pairs (<i>False positive</i>)	78 pairs
	Non-substitutable	4 pairs (<i>False negative</i>)	269 pairs (<i>True negative</i>)	273 pairs
Total		37 pairs	314 pairs	351 pairs

1 substitutability patterns extracted from computational
2 datasets. This reflects real-world scenarios where re-
3 searchers must consider all available knowledge to fill the
4 gaps raised by limited experimental data before selecting
5 candidates for expensive synthesis. Finally, after evalua-
6 ting the predictive performance across all settings, we
7 analyze the element substitutability patterns captured
8 using the multi-source approach to gain deeper insights
9 into the underlying HEA formation mechanisms of qua-
10 ternary alloys.

11 C. Materials descriptors

12 Descriptors, which are the representation of alloys,
13 play a crucial role in building a recommender system to
14 explore potential new HEAs. In this research, the raw
15 data of alloys is represented in the form of element com-
16 binations. Several descriptors have been studied in ma-
17 terials informatics to represent the compounds⁵². To em-
18 ploy the data-driven approaches for this work, we applied
19 compositional descriptor⁵³ and binary elemental descrip-
20 tor.

21 Compositional descriptors represent each alloy through
22 135 features derived from 15 atomic properties of con-
23 stituent elements. These properties include structural
24 parameters (*atomic number*, *mass*, *period*, and *group*),
25 electronic characteristics (*first ionization energy*, *second*
26 *ionization energy*, *Pauling electronegativity* and *Allen*,
27 *electronegativity*), size factors (*van der Waals*, *covalent*,
28 and *atomic radii*), and thermophysical properties (*melt-*
29 *ing point*, *boiling point*, *density*, *specific heat*). For each
30 atomic property, we calculate statistical numbers, in-
31 cluding mean, standard deviation, and pairwise covari-
32 ances across the alloy's elements, to represent the alloy.

33 The compositional descriptors can be applied not only to
34 crystalline systems but also to molecular systems. How-
35 ever, the descriptors cannot easily distinguish alloys with
36 different numbers of constituent elements, because they
37 treat the atomic properties as statistical distributions.
38 Therefore, the descriptors cannot be applied when ex-
39 trapolating to alloys with a different number of compo-
40 nents.

41 Binary elemental descriptors use binary encoding to
42 indicate element presence (1) or absence (0) in an alloy.
43 The number of binary elemental descriptors corresponds
44 to the number of element types included in the train-

45 ing data. In this study, the binary elemental descrip-
46 tors are used to represent the alloys in the DS-source,
47 LLM-source, and multi-source models. In contrast, the
48 compositional descriptors are applied for the LR-based
49 model.

50 IV. RESULTS AND DISCUSSIONS

51 A. Reliability Assessment of LLM-Based Elemental 52 Substitutability Knowledge

53 Verifying the reliability of large language model (LLM)
54 responses is a prerequisite for trusting downstream pre-
55 dictions. We therefore validate element-substitutability
56 knowledge extracted from LLM queries against the em-
57 pirical Hume–Rothery rules⁵⁴, which are a set of ba-
58 sic rules for predicting elemental substitution. These
59 rules stipulate that elements readily substitute in solid
60 solutions when: (i) atomic radius mismatch is lower
61 than 15%, (ii) they share similar crystal structures and
62 valence states, and (iii) they have similar electronega-
63 tivity. When electronegativity differences exceed criti-
64 cal thresholds, metals typically form intermetallic com-
65 pounds rather than solid solutions. For this validation,
66 we use an electronegativity difference threshold of 0.55.
67 For valency comparison in metallic alloy systems, we con-
68 sider the effective valency⁵⁵ (number of electrons effec-
69 tively contributing to metallic cohesion). While most
70 metals exhibit a single characteristic valency, certain
71 transition metals (e.g., Fe, Co, Mn, Cr) can exhibit mul-
72 tiple effective valencies in different alloy environments.
73 In our analysis, two elements are considered to have sim-
74 ilar valency if they share at least one common valence
75 state.

76 We aggregated substitutability assessments from four
77 LLMs, including Grok3, Claude Opus 4, GPT-4o, and
78 GPT-4.5, for 351 element pairs using our DST frame-
79 work. Each pair is classified as substitutable if the com-
80 bined belief for substitutability exceeds that for non-
81 substitutability. Comparison against Hume–Rothery
82 predictions reveals strong alignment: 86% of element
83 pairs show identical classifications with high recall rates
84 for substitutable labels and high precision for non-
85 substitutable labels, as shown in Table III. Specifically,
86 33 of 37 pairs (89%) deemed substitutable by Hume–
87 Rothery rules are correctly identified by LLMs, while



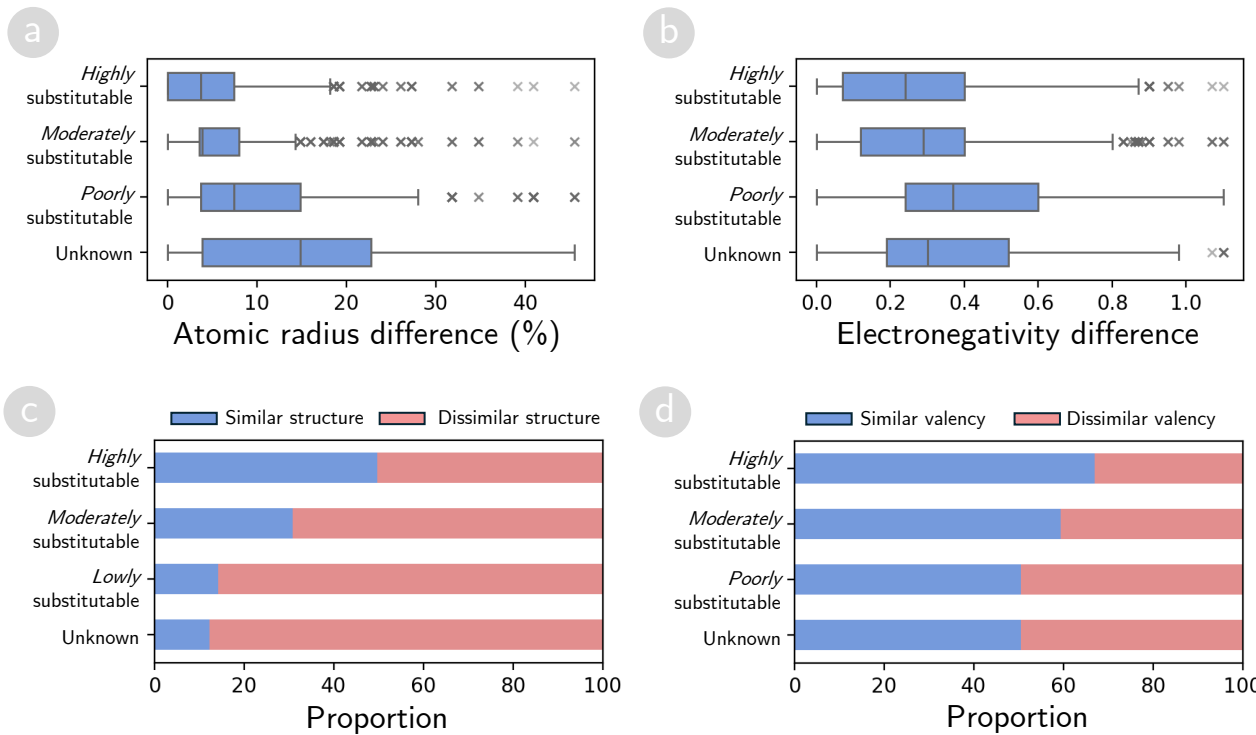


FIG. 3. Validation of LLM-extracted substitutability against Hume–Rothery rules. (a, b) Distribution of atomic radius differences (a) and electronegativity differences (b) for element pairs categorized by LLM-predicted substitutability levels (highly, moderately, and poorly substitutable, plus unknown). Box plots show median, interquartile range, and outliers. (c, d) Proportions of element pairs with similar versus dissimilar crystal structures and valency, grouped by substitutability levels.

1 269 of 273 pairs classified as non-substitutable by LLMs
2 matched Hume–Rothery rules, achieving a precision of
3 99%.

4 The 14% misalignment consists entirely of cases where
5 LLMs identify additional substitutable pairs beyond the
6 traditional Hume–Rothery criteria. Among the 45 mis-
7 aligned pairs, most satisfy the size and electronegativity
8 requirements but exceed traditional thresholds for va-
9 lency or crystal structure differences. Remarkably, ex-
10 perimental validation supports these context-specific pre-
11 dictions: 14 of these pairs have been confirmed to form
12 single-phase binary systems⁵⁶, as shown in Supplemen-
13 tary Table 3. Additionally, Cr and Nb differ in valence
14 electron counts (Cr: 6, Nb: 5), placing them outside
15 general substitutability criteria. However, when incor-
16 porated into quaternary systems, they demonstrate suc-
17 cessful substitution—Cr in quaternary system Cr-Al-Ti-V
18 can be replaced by Nb (forming Nb-Al-Ti-V), and simi-
19 larly in Cr-Ta-Ti-V and Nb-Ta-Ti-V systems, both form
20 stable single-phase BCC structures.

21 This asymmetric difference reflects a fundamental
22 distinction between general rules and context-specific
23 knowledge. The Hume–Rothery rules, developed through
24 careful empirical observation, provide general guidelines
25 with well-defined thresholds (e.g., 15% for radius dif-
26 ference) that have successfully guided alloy design for

27 decades. These universal criteria ensure high reliability
28 across diverse alloy systems. In contrast, LLMs capture
29 context-dependent substitutability documented in mate-
30 rials literature⁵⁷, in which specific processing conditions,
31 alloy compositions, or applications enable successful sub-
32 stitution despite exceeding general thresholds. LLMs in-
33 tegrate knowledge from documented experimental sys-
34 tems across material families for general substitutability
35 assessment, explaining why they complement conserva-
36 tive Hume–Rothery rules with context-specific insights.
37 Detailed analysis of all 45 pairs with experimental vali-
38 dation status is provided in Supplementary Table 3.

39 Figure 3 analyzes in detail the alignment of LLM’s re-
40 sponse with each criterion of substitutability from Hume–
41 Rothery rules. Element pairs that LLMs identified as
42 highly substitutable exhibit significantly lower atomic
43 radius differences and electronegativity differences com-
44 pared to pairs identified as poorly substitutable, as shown
45 in Figure 3(a-b). Additionally, highly substitutable pairs
46 predominantly share similar crystal structures and valen-
47 cies, while poorly substitutable pairs rarely do as shown
48 in Figure 3(c-d).

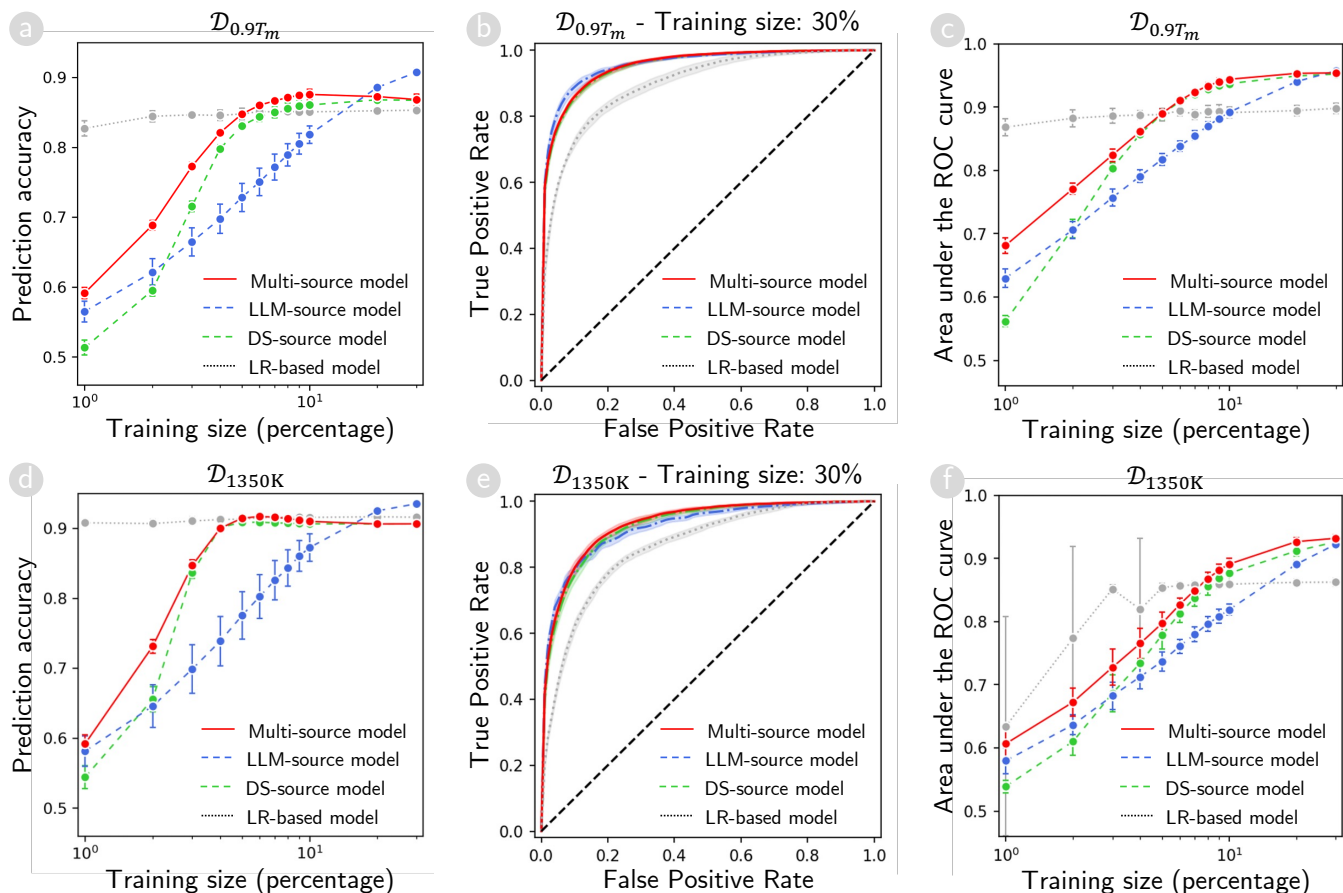


FIG. 4. Predictive capability evaluation via cross-validation on quaternary-alloy datasets $\mathcal{D}_{0.9T_m}$ and \mathcal{D}_{1350K} . (a, d) Classification accuracy of the multi-source, single-source, and LR-based models on two quaternary-alloy datasets $\mathcal{D}_{0.9T_m}$ and \mathcal{D}_{1350K} . (b, e) Receiver operating characteristic (ROC) curves for the same models at a 30% training-set size on these datasets. (c, f) Area under the ROC curves (AUC) for each model across different training-set sizes, providing an overall measure of discriminative performance. In all subplots, red lines indicate the multi-source model (using both DS and LLM sources), green and blue lines represent single-source models (using either DS or LLM sources), and gray lines represent the LR-based model.

1 B. Cross-Validation Analysis of Multi-Source Knowledge 2 Integration

3 For the experiment, we systematically vary the train-
4 ing set size from 1% to 30% of each quaternary-alloy
5 dataset, incrementing by 1% up to 10%, followed by steps
6 of 20% and 30%. The variation enables the assessment of
7 how different methods handle data scarcity versus mod-
8 erate availability.

9 Figures 4(a,d) and 5(a,d) show the classification ac-
10 curacy of the single-source, multi-source, and LR-based
11 models on the four datasets. At smaller training sizes
12 (approximately 1%–10%), the LR-based model achieves
13 the highest overall accuracy, outperforming evidential
14 models, which explicitly model element substitutabil-
15 ity to predict alloy properties. Among the evidential
16 models, single-source LLM models initially outperform
17 DS-source models, attributed to LLM-derived domain-
18 specific insights that assist in mitigating data limita-

19 tions. However, multi-source models remain competitive
20 and sometimes achieve the highest accuracy among evi-
21 dential models, even with limited data. As the training
22 size exceeds 10%, DS-source models exhibit superior per-
23 formance on the magnetization and Curie temperature
24 datasets while achieving comparable accuracy to LLM-
25 source models on alloy stability datasets. Conversely,
26 the accuracy of LR-based models plateaus and is even-
27 tually outperformed by evidential models. These find-
28 ings underscore the importance of incorporating LLM-
29 based, DS-source, or multi-source knowledge to improve
30 quaternary-alloy property predictions.

31 Although prediction accuracy provides a convenient
32 single-metric overview, it relies on a fixed classification
33 threshold (typically 0.5), which may not be optimal for
34 imbalanced datasets, where HEAs (positive class) are rel-
35 atively rare. Under these conditions, LR-based models
36 may serve effectively at extremely small training sizes
37 when they effectively predict the dominant (Non-HEA)
38 class by default, thereby inflating accuracy. However,

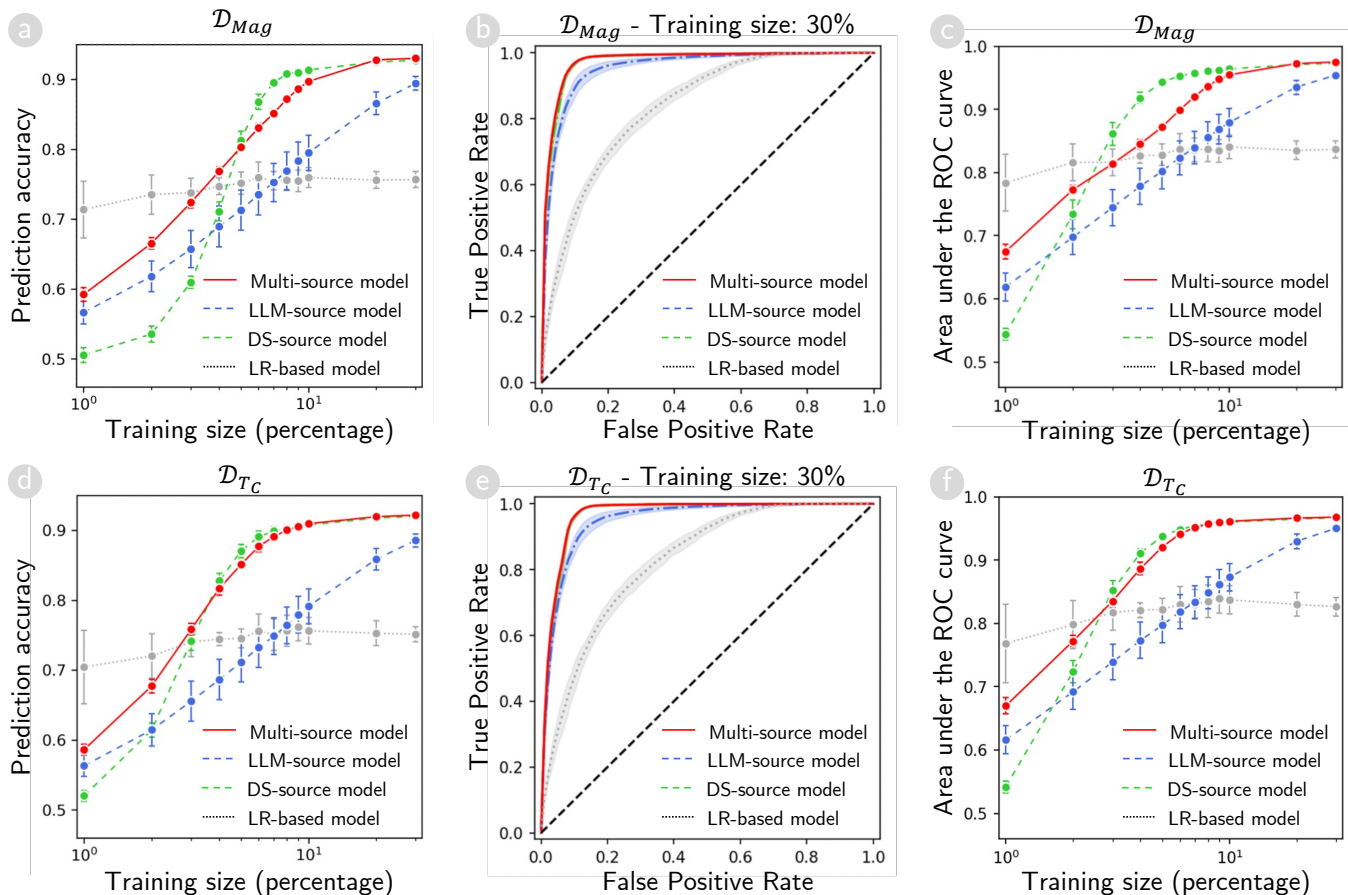


FIG. 5. Predictive capability evaluation via cross-validation on quaternary-alloy datasets \mathcal{D}_{Mag} and \mathcal{D}_{TC} . (a, d) Classification accuracy of the multi-source, single-source, and LR-based models on two quaternary alloy datasets \mathcal{D}_{Mag} and \mathcal{D}_{TC} . (b, e) Receiver operating characteristic (ROC) curves for the same models at a 30% training-set size on these datasets. (c, f) Area under the ROC curves (AUC) for each model across different training-set sizes, providing an overall measure of discriminative performance. In all subplots, red lines indicate the multi-source model (using both DS and LLM sources), green and blue lines represent single-source models (using either DS or LLM sources), and gray lines represent the LR-based model.

1 this approach fails to address scenarios where different
 2 types of misclassifications (false positives versus false neg-
 3 atives) incur different costs.

4 To effectively capture these trade-offs under dynamic
 5 thresholds, we analyze receiver operating characteristic
 6 (ROC) curves across the four datasets, which illustrate
 7 variations in true positive rate (TPR) and false positive
 8 rate (FPR) of each model across all possible decision
 9 boundaries. Figures 4(b,e) and 5(b,e) depict the ROC
 10 curves for the multi-source models, LLM-source models,
 11 DS-source models, and LR-based models at a 30% train-
 12 ing size. Overall, the multi-source and DS-source mod-
 13 els exhibit comparable ROC performance and outper-
 14 form the other models. The LLM-source models achieve
 15 results comparable to the best ones on the alloy sta-
 16 bility datasets $\mathcal{D}_{0.9T_m}$ and $\mathcal{D}_{1350\text{K}}$ but lag behind DS-
 17 source models on the magnetization and Curie tempera-
 18 ture datasets \mathcal{D}_{Mag} and \mathcal{D}_{TC} . Therefore, knowledge col-
 19 lected from the five considered research domains may
 20 not fully capture the magnetic and thermal properties

21 reflected in those datasets. Meanwhile, the LR-based
 22 models consistently show the lowest performance across
 23 all four datasets.

24 To further assess the ROC performance of each model
 25 at different training sizes, we analyze the AUC distri-
 26 bution from 1% to 30% training data, as shown in Fig-
 27 ures 4(c,f) and 5(c,f). When the training set is extremely
 28 small, LLM-based models generally attain an early ad-
 29 vantage, presumably because domain insights compen-
 30 sate for limited alloy observations. However, as data ac-
 31 cumulates, DS-source models typically outperform LLM-
 32 source models, suggesting that direct data-driven cues
 33 from quaternary-alloy datasets become increasingly de-
 34 cisive. In contrast, multi-source models maintain robust
 35 performance across all training sizes, benefitting from
 36 their ability to merge domain-specific substitutability in-
 37 sights with empirical data. Multi-source models leverage
 38 complementary evidence, enabling an effective balance
 39 between TPR and FPR. On stability datasets $\mathcal{D}_{0.9T_m}$ and
 40 $\mathcal{D}_{1350\text{K}}$, DS-source and multi-source models achieve com-

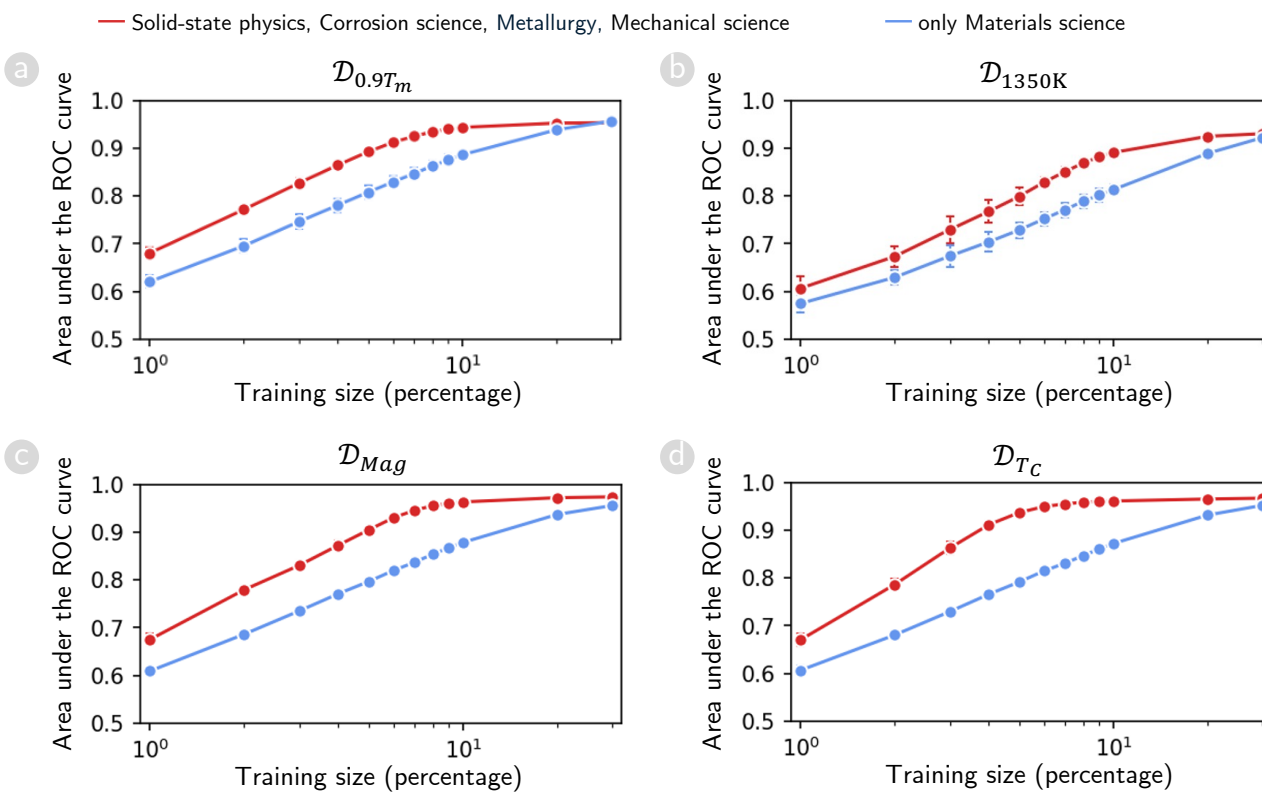


FIG. 6. Performance comparison of explicit versus implicit domain integration. Area under ROC curves for predicting HEA stability ($\mathcal{D}_{0.9T_m}$, \mathcal{D}_{1350K}) and magnetic properties (\mathcal{D}_{Mag} , \mathcal{D}_{Tc}) using two domain integration strategies: (i) systematic combination of four specialized domains (solid-state physics, corrosion science, metallurgy, materials mechanics) shown in red, (ii) only using materials science, which serves as an integrative field that synthesizes perspectives from four specialized domains, shown in blue.

parable AUC early on and remain highly competitive as training data accumulates. For magnetization and Curie-temperature datasets, DS-source models briefly outperform multi-source models at moderate training sizes (approximately 6–20%), but this gap diminishes at larger training sizes.

We note that the LLM-derived substitutability matrix \mathbf{M} remains fixed across all training sizes (LLMs are used out-of-the-box without retraining); improved performance with larger training sets results from having more host compositions available to apply this fixed knowledge through substitution-based inference (Section II.D). This explains why LLM-source and multi-source models benefit from increased training data despite the LLM knowledge itself remaining unchanged.

Figure 6 provides compelling evidence for the effectiveness of our systematic evidence combination approach compared to relying on materials science as an integrative domain that synthesizes perspectives from the other four domains. Significantly, using only materials science knowledge yields substantially lower performance by 10–20% across all datasets than our multi-source framework, which systematically combines evidence from the four

specialized domains, across different prediction tasks.

This performance gap demonstrates the fundamental advantage of our Dempster–Shafer-based approach: while materials science provides a static, pre-integrated perspective that may obscure domain-specific nuances, our framework preserves distinct domain insights and adaptively weights them based on their alignment with target properties. The superior performance of our systematic combination method validates that explicit, property-aware evidence synthesis outperforms implicit knowledge fusion, particularly when different domains contribute varying degrees of relevant information for specific material properties such as stability, magnetization, or Curie temperature.

While LLM-source models generally perform well, our results reveal two scenarios where they potentially underperform compared to data-driven approaches.

1. *Property-specific predictions with weak domain alignment:* For magnetic property datasets (\mathcal{D}_{Mag} , \mathcal{D}_{Tc}), DS-source substantially outperforms LLM-source, showing a larger performance gap than observed for phase stability datasets (Figures 4 and 5). The five selected domains (corrosion

TABLE IV. Prediction accuracy and Areas under the receiver operating characteristic (ROC) curves of various methods on quaternary-alloy datasets in extrapolation experiments. For each dataset, alloys containing a specific element e are systematically excluded from the training set and used exclusively for testing. Results are reported as mean accuracy and mean AUC, averaged across all elements e within each dataset, with standard deviations reflecting variability across elements.

Evaluation criteria	Methods	$\mathcal{D}_{0.9T_m}$	\mathcal{D}_{1350K}	\mathcal{D}_{Mag}	\mathcal{D}_{T_C}
Prediction accuracy	Multi-source model	0.86 ± 0.06	0.92 ± 0.04	0.86 ± 0.19	0.86 ± 0.18
	LLM-source model	0.84 ± 0.09	0.90 ± 0.09	0.81 ± 0.21	0.86 ± 0.18
	DS-source model	0.50 ± 0.04	0.51 ± 0.05	0.48 ± 0.07	0.50 ± 0.10
	LR-based model	0.83 ± 0.05	0.91 ± 0.04	0.67 ± 0.15	0.68 ± 0.13
Area under ROC curves	Multi-source model	0.93 ± 0.06	0.92 ± 0.08	0.95 ± 0.06	0.94 ± 0.07
	LLM-source model	0.91 ± 0.11	0.90 ± 0.12	0.95 ± 0.06	0.94 ± 0.07
	DS-source model	0.50 ± 0.00	0.50 ± 0.00	0.50 ± 0.00	0.50 ± 0.00
	LR-based model	0.85 ± 0.11	0.82 ± 0.10	0.84 ± 0.06	0.84 ± 0.06

science, materials mechanics, metallurgy, solid-state physics, materials science) were optimized for structural stability and do not adequately capture magnetic exchange interactions or spin configurations.

2. *Data-rich regimes*: At large training sizes ($>20\%$, Figures 4 and 5), DS-source matches or exceeds LLM-source performance across all datasets. When sufficient data exists, empirical patterns extracted directly from the dataset provide adequate information, and general domain knowledge offers minimal additional value.

In conclusion, LLM-source models excel in data-scarce scenarios by leveraging domain-specific insights to mitigate sparsity-related challenges. As data availability increases, DS-source models outperform LLM-source models, particularly where DS-derived evidence provides sufficient information for a purely data-driven learning approach. Multi-source models, which integrate insights derived from LLM and DS-sources, demonstrate robust and consistent performance across various training sizes.

C. Extrapolation Analysis of Multi-Source Knowledge Integration

Having assessed the proposed framework via cross-validation (Section IV B), we examine its *extrapolation* performance on quaternary alloys containing an element e , which is excluded during training. Unlike the cross-validation experiments, the training set size is not varied for this set of experiments. Instead, for each element e , we remove all e -containing alloys from the dataset and train each model on the remaining alloys that do not contain e . Further, we evaluate the ability of the models to predict the properties of e -containing alloys. This procedure tests whether the learned models can generalize to compositions containing unseen elements in their training datasets.

Table IV reveals distinct performance patterns across model types. DS-source models fail in this scenario,

achieving ~ 0.50 accuracy (random guessing) across all datasets because they cannot extract substitutability patterns for absent element e from training data. In contrast, LLM-source models achieve substantially higher accuracies across all datasets. Multi-source models modestly outperform LLM-source on phase stability datasets ($\mathcal{D}_{0.9T_m}$ and \mathcal{D}_{1350K}) but achieve nearly identical performance on magnetic property datasets (\mathcal{D}_{Mag} and \mathcal{D}_{T_C}). This convergence of multi-source and LLM-source performance on magnetic datasets reflects proper uncertainty handling rather than a limitation. When element e is absent from training, DS-source has no observed substitutability patterns involving e . Following the principle established in Section II A, DS-source assigns unit mass to the uncertainty set, explicitly representing total ignorance about e -containing compositions. When this total uncertainty combines with confident LLM evidence through Dempster's rule (Equation 7), the final multi-source prediction is naturally dominated by informative LLM knowledge. The framework thus explicitly represents *unknown* rather than forcing unreliable predictions from insufficient data, demonstrating principled uncertainty quantification in extrapolation scenarios.

Figure 7 illustrates the ROC curves, showing that the multi-source and LLM-source models consistently exhibit higher TPR at comparable FPR across all datasets. Conversely, DS-source models exhibit near-random discrimination, as evidenced by their diagonal ROC curves, while LR-based models yield moderate performance between these extremes. To quantify these visual differences, Table IV also lists AUC for each dataset. Multi-source models achieve the highest AUC scores (0.92–0.95), followed closely by LLM-source models (0.90–0.95), while LR-based models peak at approximately 0.85, and DS-source models hover at approximately 0.50.

Figure 8a–c illustrates knowledge integration in extrapolation simulations for Os-based alloys using the $\mathcal{D}_{0.9T_m}$ dataset. Specifically, Figures 8a and 8b present maps reconstructed from element substitutability patterns derived from the DS-source and multi-source models, respectively, both trained on $\mathcal{D}_{0.9T_m}$ dataset excluding Os-based alloys. Details of the visualization method



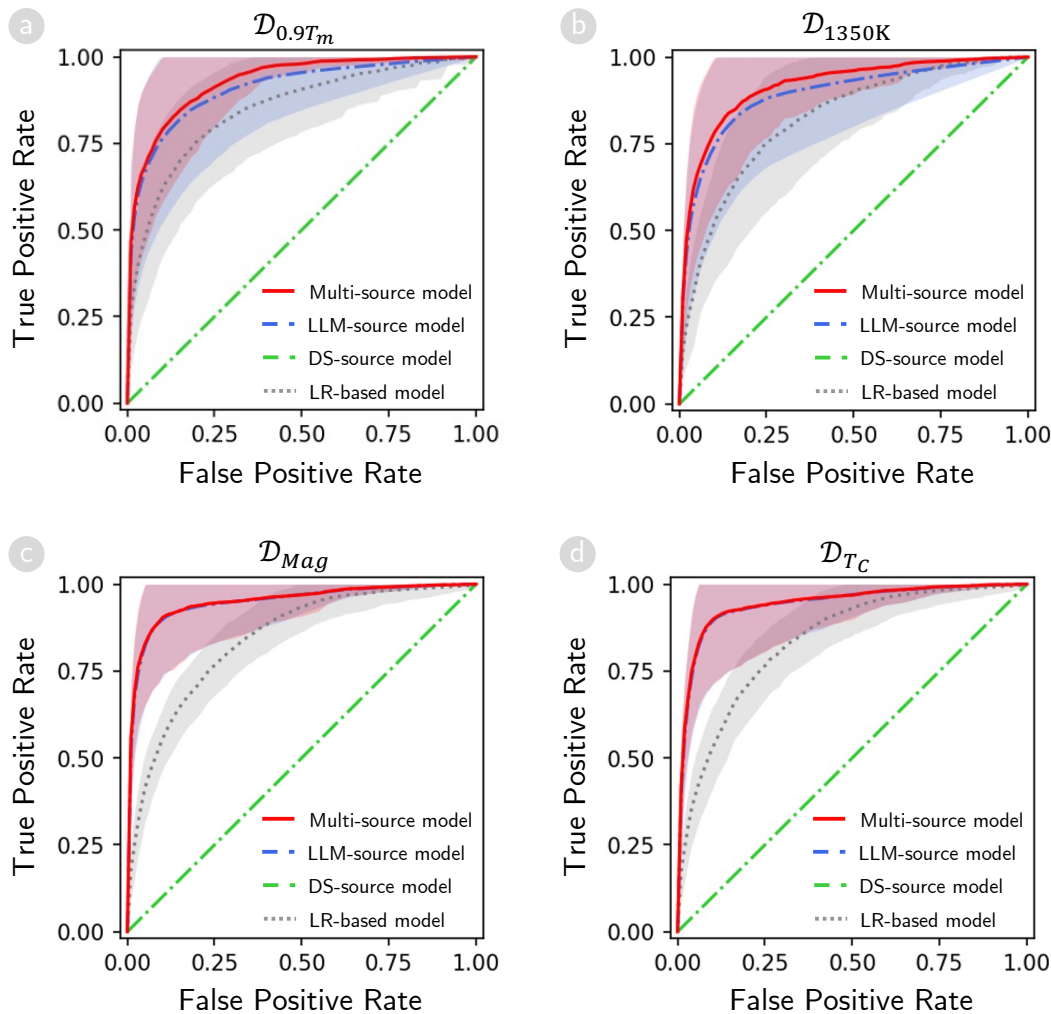


FIG. 7. Predictive capability evaluation via extrapolation on quaternary-alloy datasets. For each dataset, alloys containing a specific element e are systematically excluded from the training set and used exclusively for testing. (a–d) Area under the receiver operating characteristic (ROC) curves (AUC) is plotted for each model on their respective test sets in the extrapolation experiments. In all subplots, red lines represent the multi-source model (integrating both DS and LLM sources), green and blue lines represent single-source models (using either DS or LLM sources), and gray lines represent the LR-based model.

are shown in Supplementary Section 4. In these visualizations, the observed alloys are well-structured into sub-clusters according to their phase formation behavior, with blue markers indicating HEA-forming alloys and red markers representing non-HEA alloys. The Os-based candidate alloys, depicted as white circular markers, consistently form a distinct sub-cluster in the upper region of each map. In these visualizations, the background coloration indicates the predicted probability of HEA formation, with deeper blue regions suggesting higher probability of forming stable HEAs.

The limitations of the DS-source model become evident in Figure 8a, where the phase behavior of Os-based alloys remains undetermined due to the absence of Os-

containing alloys in the training dataset. This knowledge gap leaves researchers with no guidance when exploring the uncharted territory of Os-based alloys, forcing them to rely on random selection. In contrast, our multi-source approach addresses this limitation by integrating expert insights distilled from scientific literature using LLMs, as illustrated in Figure 8b. The effectiveness of this approach is visually confirmed in Figure 8c, where the multi-source model's predictions closely align with the actual phase behavior of the candidates. This qualitative assessment is complemented by quantitative evaluation in Supplementary Table 4, which reports that the multi-source model achieves an impressive 88% prediction accuracy for Os-based alloys, validating our approach's ca-

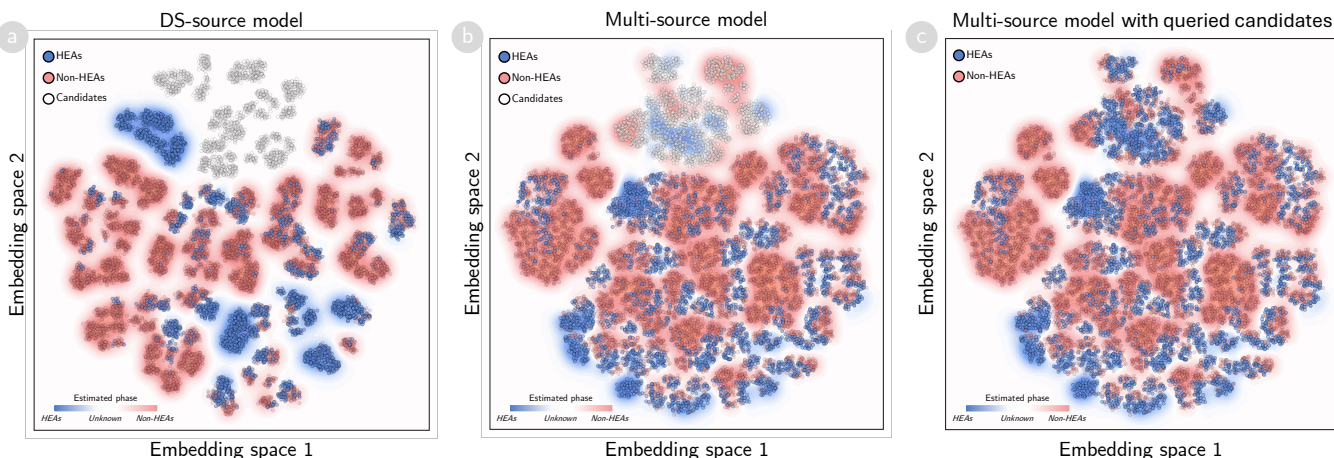


FIG. 8. **Visualization of Os-based alloy extrapolation in dataset $\mathcal{D}_{0.9T_m}$.** (a) Alloy map generated from element substitutability patterns extracted using the DS-source model after excluding Os-based alloys from training. (b–c) Alloy maps generated from element substitutability patterns extracted using the multi-source model after excluding Os-based alloys from training. The map in (c) incorporates queried labels for Os-based candidate alloys. Marker colors represent phase formation: blue for HEA alloys, red for non-HEA alloys, and white for Os-based candidate alloys. Background coloration indicates the predicted phase formation probability according to the DS-source model (a) and multi-source model (b–c), with deeper blue shades suggesting higher probability of HEA formation.

1 pability to effectively extrapolate to unexplored compo-
2 sitional spaces. In summary, these results confirm that
3 leveraging multi-source or LLM-based evidence signifi-
4 cantly enhances discriminative power in the extrapolation
5 scenario.

6 D. Effectiveness Assessment on Experimental High-Entropy 7 Alloy Data

8 To assess the real-world applicability of our frame-
9 work, we validated its performance on experimentally
10 verified alloys from the literature. This validation ex-
11 amines whether the proposed framework, developed pri-
12 marily using computational datasets, can accurately pre-
13 dict phase stability for experimentally synthesized al-
14 loys. Our framework integrates LLM-derived knowledge
15 with substitutability patterns extracted from computa-
16 tional databases using the methodology described in Sec-
17 tion II A. This reflects real-world scenarios where re-
18 searchers must consider all available knowledge before
19 selecting candidates for expensive synthesis.

20 We performed 5-fold cross-validation on experimental
21 datasets: $\mathcal{D}_{\text{HEA}}^{\text{exp}}$ of 55 experimentally confirmed alloys.
22 For the HEA dataset $\mathcal{D}_{\text{HEA}}^{\text{exp}}$, we integrated LLM knowl-
23 edge with substitutability patterns extracted from com-
24 putational datasets \mathcal{D}_{1350K} , $\mathcal{D}_{\text{AFLOW}}$, $\mathcal{D}_{\text{CALPHAD}}$, and
25 $\mathcal{D}_{\text{LTVC}}$. Details of the computational datasets are in-
26 troduced in the Supplementary Section 6. Notably, the
27 predictions from these computational methods for the 55
28 experimentally confirmed alloys are not utilized in our
29 framework training, ensuring unbiased validation.

30 For benchmarking on the HEA dataset, we compared

31 our framework against four empirical rules (ERs)^{58–61},
32 two free-energy models (FEM)^{3,62}, and a valence-electron
33 concentration (VEC) model⁶³. Supplementary Table 2
34 provides details of these baseline models. Addition-
35 ally, we compared our framework with results obtained
36 from computational datasets $\mathcal{D}_{\text{AFLOW}}$ ¹⁵, $\mathcal{D}_{\text{LTVC}}$ ¹⁹, and
37 \mathcal{D}_{1350K} ⁴⁵. These computational datasets are collected
38 by using high-throughput approaches and Hamiltonian
39 models.

40 Figure 9a presents ROC curves demonstrating that
41 our multi-source integration framework consistently out-
42 performs empirical phase selection models such as ERs,
43 FEMs, and VEC, while achieving performance compa-
44 rable to costly computational methods. These results
45 confirm that systematically integrating diverse evidence
46 sources through our DST framework enhances prediction
47 accuracy across different material classes. The frame-
48 work's value does not lie in replacing established meth-
49 ods but in effectively combining their complementary
50 strengths, creating a unified platform that enhances prac-
51 tical decision-making in materials discovery.

52 To investigate the underlying mechanisms of forming
53 HEAs, we analyzed the elemental substitutability pat-
54 terns extracted by our framework from multiple evidence
55 sources. Specifically, we integrated substitutability infor-
56 mation from the experimental dataset $\mathcal{D}_{\text{HEA}}^{\text{exp}}$, computa-
57 tional datasets (\mathcal{D}_{1350K} , $\mathcal{D}_{\text{AFLOW}}$, $\mathcal{D}_{\text{CALPHAD}}$, $\mathcal{D}_{\text{LTVC}}$),
58 and LLM-derived knowledge.

59 Figure 9b presents the substitutability matrix for 26
60 elements relevant to HEA stability, along with their hi-
61 erarchical clustering structure. The dendrogram is gen-
62 erated via hierarchical agglomerative clustering (HAC)
63 with the complete linkage criterion, grouping elements

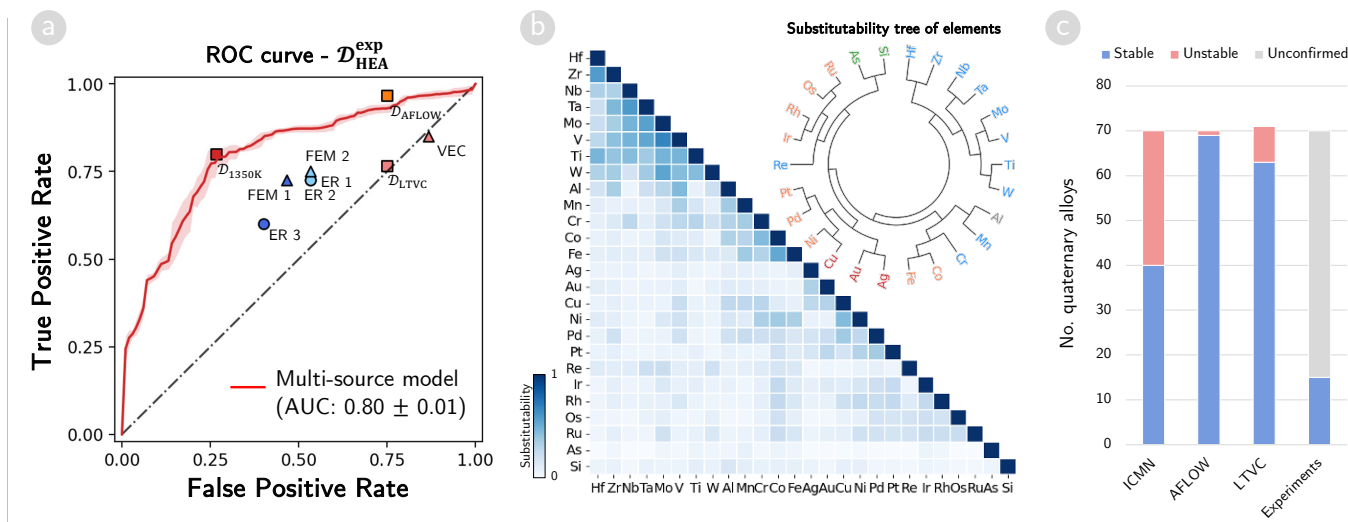


FIG. 9. Effectiveness Assessment of Multi-Source Knowledge Integration for High-Entropy Alloy Formation. (a) Receiver operating characteristic (ROC) curves for the phase estimation task on experimental dataset $D_{\text{HEA}}^{\text{exp}}$. Red line represent the multi-source model (integrating both DS and LLM sources) and gray dashed line represent the random selection. Coloured scatter points represent results of ERs, FEMs, VEC, and computational methods that return only a single stable/unstable estimation. (b) Substitutability matrix and substitutability tree for 26 elements. Matrix values represent substitutability scores derived from integrated computational datasets, experimental dataset and LLM sources. The substitutability tree is generated using hierarchical agglomerative clustering with complete linkage criterion. Element colors: blue (early transition metals), orange (intermediate transition metals), gray (post-transition elements). (c) Predicted phase stability for 70 possible quaternary alloys from Group 1 elements (Hf, Zr, Nb, Ta, Mo, V, Ti, W). Bars show number of alloys predicted as single-phase obtained from computational datasets (D_{AFLOW}^{15} , D_{LTVC}^{19} , and $D_{1350\text{K}}^{45}$) and experimentally verified single-phase HEAs^{45,49,50}.

1 based on similar substitutability patterns. The substitutability analysis reveals three distinct element groups 2 with strong intra-group substitutability. Group 1 3 comprises eight early transition metals from periodic groups 4–6: Ti, Zr, Hf (group 4); V, Nb, Ta (group 5); and Mo, 5 W (group 6). Cr, while belonging to group 6, exhibits 6 unique behavior, showing moderate substitutability with 7 Group 1 elements but high substitutability with Fe, Co, 8 Mn, and Al, which together form Group 2. Group 3 9 contains primarily late transition metals from periodic 10 groups 9–11, including Rh, Ir, Pd, Pt, Ni, Cu, Au, Ag. 11 Notably, Groups 1 and 3 show weak inter-group substitutability 12 but moderate substitutability with the bridging Group 2. 13

14 The exceptional intra-group substitutability of Group 15 elements (Ti, Zr, Hf, V, Nb, Ta, Mo, W), exhibiting 16 notably higher scores than Groups 2 and 3, suggests a 17 design principle: quaternary combinations should readily 18 form stable single-phase HEAs. Critically, this substitutability 19 matrix (Figure 9b) is derived by fusing evidence from 20 multiple independent sources—experimental HEA dataset ($D_{\text{HEA}}^{\text{exp}}$), computational databases ($D_{1350\text{K}}$, 21 D_{AFLOW} , D_{LTVC}), and 20 LLM-domain sources—through 22 Dempster–Shafer integration; such high mutual substitutability 23 indicates unanimous agreement across all 24 sources regarding these patterns. Figure 9c validates 25 this prediction: all three computational datasets unanimously 26 predict single-phase formation for all 70 possible

27 Group 1 quaternaries, and all 15 experimentally synthesized 28 compositions form single-phase HEAs (100% success rate). 29 This agreement is consistent with established principles 30 for refractory high-entropy alloys^{41,64}: early transition 31 metals (groups 4–6) preferentially form stable BCC solid 32 solutions due to similar atomic sizes and compatible 33 electronic structures, with single-phase stability 34 thermodynamically reinforced by configurational entropy 35 that lowers Gibbs free energy at elevated temperatures⁶⁵.

38 E. Effectiveness Assessment on Experimental High-Entropy 39 Boride Data

40 We extend our analysis to high-entropy borides 41 (HEBs), where boron's restrictive bonding requirements 42 create similarly high elemental selectivity as observed in 43 HEAs⁶⁶. Despite different underlying mechanisms, both 44 systems share the key challenge of identifying rare viable 45 combinations within vast compositional spaces, making 46 HEBs suitable for demonstrating our framework's applicability 47 to diverse multi-component materials with stringent 48 compatibility constraints.

49 In this experiment, we applied our framework to a 50 dataset of 19 experimentally confirmed quinary borides 51 collected from previous studies. Using these validated 52 compositions as training data, our framework was then 53 employed to rank 314 potential quinary boride candi-

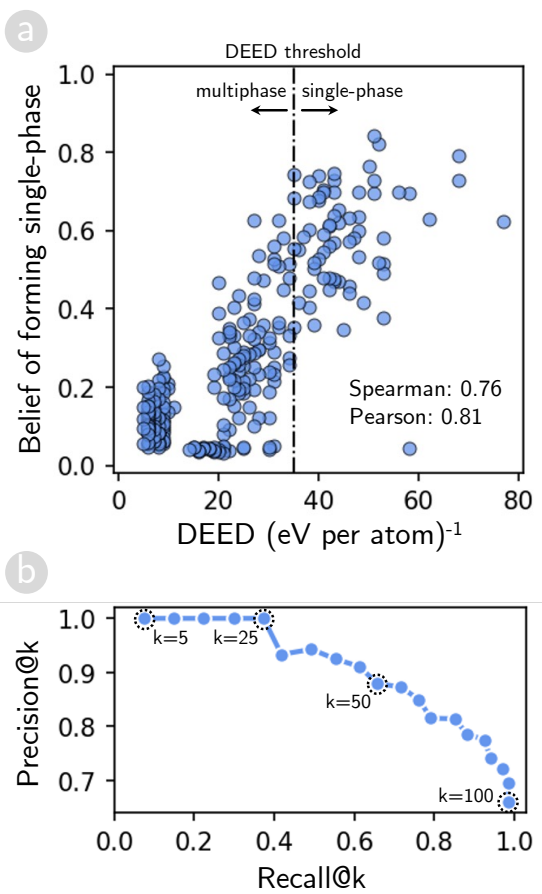


FIG. 10. Effectiveness Assessment of Multi-Source Knowledge Integration for High-Entropy Borides Formation. (a) Correlation analysis between our framework's single-phase formation belief and the disordered enthalpy-entropy descriptors (DEED) for 275 quinary boride candidates. The dashed line indicates the DEED threshold of $35 \text{ (eV per atom)}^{-1}$ for single-phase prediction. (b) Precision@ k and Recall@ k performance metrics evaluated at k values from 5 to 100 with increments of 5

dates formed by boron as the anion and the following 2 metals: Cr, Hf, Ir, Mn, Mo, Nb, Ta, Ti, V, W, Y, Zr. To 3 benchmark our framework, we compared the rankings 4 obtained by our framework with those derived using the 5 disordered enthalpy-entropy descriptors (DEED)⁴⁴, which 6 represents the state-of-the-art descriptor based on ab- 7 initio calculations for guiding experimental discovery of 8 new single-phase high-entropy carbonitrides and borides.

Figure 10a illustrates the correlation between DEED 10 values and the belief of forming single-phase structures 11 for 275 of the 314 quinary boride candidates. For the 12 remaining 39 candidates, our framework could not pro- 13 vide reliable predictions due to insufficient training data 14 coverage, resulting in maximum uncertainty values that 15 rendered these predictions uninformative for comparison

16 purposes. The results demonstrate a strong positive lin- 17 ear correlation between the single-phase formation belief 18 derived from our framework and the DEED values, with 19 Pearson and Spearman correlation coefficients of 0.81 and 20 0.76, respectively. The previous DEED study established 21 a threshold of $35 \text{ (eV per atom)}^{-1}$ to distinguish be- 22 tween single-phase and multiphase candidates, where val- 23 ues above this threshold indicate predicted single-phase 24 formation.

25 The strong correlation for the 275 confident predic- 26 tions, combined with explicit uncertainty flagging for 39 27 candidates, demonstrates effective uncertainty quantifi- 28 cation. To further validate this mechanism, we analyzed 29 prediction accuracy at varying uncertainty thresholds, as 30 shown in Supplementary Figure 8. The results reveal 31 a systematic trade-off: as the uncertainty threshold de- 32 creases (accepting more uncertain predictions as confi- 33 dent), prediction accuracy degrades accordingly. This 34 behavior confirms that high uncertainty values success- 35 fully flag regions where evidence is insufficient, prevent- 36 ing overconfident extrapolation beyond the training data. 37 The explicit uncertainty quantification thus serves as a 38 critical safeguard against overfitting in data-sparse sce- 39 narios, distinguishing our approach from conventional 40 machine learning methods that would force predictions 41 regardless of data sufficiency.

42 To evaluate our framework's practical utility as a ma- 43 terials discovery tool, we analyzed how well it ranks 44 promising candidates compared to the established DEED 45 method. We measured this using standard ranking met- 46 rics: Precision@ k (what percentage of our top k recom- 47 mendations are actually good) and Recall@ k (what per- 48 centage of all good candidates we capture in our top k 49 recommendations). The results show impressive perfor- 50 mance: when we look at our top 25 recommendations 51 ($k=25$), all of them were also predicted to form single- 52 phase structures by the DEED method, giving us perfect 53 precision, as shown in Figure 10b. More broadly, to cap- 54 ture 50% of all the promising candidates identified by 55 DEED, our method requires selecting approximately the 56 top 35-40 candidates and maintains over 90% precision, 57 meaning that more than 90% of these top-ranked can- 58 didates are correctly identified as single-phase according 59 to DEED. Even when capturing 75% of the promising 60 candidates, our precision remains above 85%. These re- 61 sults demonstrate that our framework effectively priori- 62 tizes the most promising compositions for experimental 63 synthesis.

64 The strong performance on high-entropy borides, com- 65 bined with the previous results on high-entropy alloys, 66 establishes the framework's capability to handle uncer- 67 tainty in compositionally selective multi-component ma- 68 terial systems. Notably, while computational databases 69 such as AFLOW and CALPHAD carry inherent uncer- 70 tainties from DFT approximations and thermodynamic 71 extrapolations¹⁸, the Dempster–Shafer theory explicitly 72 models these through mass assignments to ignorance, 73 enabling robust integration with experimental data and



1 mitigating risks of systematic errors in guiding alloy syn-
 2 thesis. The discount factor mechanism (Equations 5–7)
 3 automatically downweights unreliable sources based on
 4 cross-validation performance, preventing error propaga-
 5 tion by allowing high-quality evidence to dominate when
 6 computational predictions conflict with experimental ob-
 7 servations.

8

9 F. Limitations and Future Extensions

10 Previous sections have demonstrated the framework's
 11 effectiveness across computational and experimental
 12 datasets. We now examine its current limitations and
 13 corresponding opportunities for future development.

14

15 *Context-Independent Evidence Weighting:* The cur-
 16 rent implementation employs fixed weighting parameters
 17 for each source without considering the specific context
 18 of elemental substitution. For instance, metallurgical
 19 knowledge may be more reliable for refractory elements,
 20 while solid-state physics insights may better inform no-
 21 ble metal substitutability. Future extensions could im-
 22 plement context-dependent weighting, wherein discount
 23 factors vary based on the element pair under consid-
 24 eration. This could be achieved by conditioning dis-
 25 count factors on elemental properties such as atomic ra-
 26 dius, electronegativity, or periodic group membership,
 27 enabling the framework to recognize element-specific re-
 28 liability patterns across different knowledge sources.

29

30 *From Uncertainty Quantification to Discovery Navi-
 31 gation:* This study proposes a framework to integrate
 32 multi-source knowledge and quantify uncertainty for can-
 33 didate materials. However, a subsequent challenge re-
 34 mains: how to effectively utilize these uncertainty mea-
 35 sures to select candidates for experimental validation un-
 36 der limited resources. This candidate selection problem
 37 inherently involves balancing exploration (investigating
 38 compositions with high uncertainty that may reveal novel
 39 alloys) and exploitation (refining predictions in promis-
 40 ing regions with moderate uncertainty). Active learning
 41 provides a principled approach to this challenge by iden-
 42 tifying experiments that maximally reduce epistemic un-
 43 certainty, prioritizing candidates where additional data
 44 would most improve model reliability. Reinforcement
 45 learning complements this by learning optimal selection
 46 policies through iterative experimental feedback, dynam-
 47 ically adjusting the exploration–exploitation balance as
 48 the discovery campaign progresses. Together, these tech-
 49 niques could transform the current prediction framework
 50 into a comprehensive decision-support system for accel-
 51 erated materials discovery.

52

53 *Symmetric Substitutability Assumption:* The sym-
 54 metric substitutability assumption ($A \rightarrow B$ and $B \leftarrow A$ are
 55 equivalent) represents a context-averaged approximation

56 that may limit accuracy for systems with strong direc-
 57 tional substitution preferences. This symmetric treat-
 58 ment is justified in this study by two factors: first, the
 59 limited training data in our data-sparse scenarios makes
 60 learning separate directional patterns statistically infea-
 61 sible; second, for near-equatomic multi-principal element
 62 HEAs characterized by disordered random solid solu-
 63 tions, elements occupy statistically similar local envi-
 64 ronments, rendering symmetric substitution a physically
 65 reasonable first-order approximation. Future extensions
 66 could incorporate asymmetric substitutability by main-
 67 taining separate $A \rightarrow B$ and $B \leftarrow A$ matrices and collect-
 68 ing directional evidence from LLMs through modified
 69 prompts.

70 *Broaden Scope Beyond Phase Stability:* To serve the
 71 purpose of screening the element combinations forming
 72 HEA phases, the proposed framework focuses on the fun-
 73 damental question of whether the HEA phase exists. We
 74 design a frame of discernment $\Omega_{HEA} = \{HEA, \overline{HEA}\}$ to
 75 model the existence of HEA phases with mass functions.
 76 Consequently, our framework has not answered essential
 77 questions regarding the structure and other properties of
 78 the HEAs. However, by redesigning the frame of discern-
 79 ment to reflect the additional properties of interest, we
 80 can also construct a model that can recommend poten-
 81 tial alloys forming HEA phases with desirable properties.
 82 Extending to mechanical, electronic, or catalytic proper-
 83 ties represents another promising direction as sufficient
 84 property-specific data becomes available⁶⁷.

85 *Scalability to Higher-Order Systems:* The current val-
 86 idation focuses primarily on quaternary alloy systems,
 87 with limited exploration of higher-order compositions.
 88 Extension to quinary and higher-order alloys could be
 89 achieved through hierarchical decomposition, wherein
 90 quaternary systems serve as baseline evidence augmented
 91 by pairwise substitutability relationships. However, more
 92 complex systems may require sparse approximation tech-
 93 niques and substantially larger materials databases to
 94 maintain predictive reliability.

95 V. CONCLUSIONS

96 The central contribution of this work lies in demon-
 97 strating that the interpolation–extrapolation dichotomy
 98 inherent to conventional data-driven materials discovery
 99 can be systematically addressed through principled inte-
 100 gration of multi-source knowledge. Crucially, the frame-
 101 work does not indiscriminately combine all available ev-
 102 idence; rather, it evaluates the reliability of each source
 103 based on its alignment with the target property, en-
 104 suring that only relevant domain knowledge contributes
 105 meaningfully to predictions. By employing elemental
 106 substitutability as a unifying concept and leveraging
 107 Dempster–Shafer theory to combine empirical observa-
 108 tions with insights extracted from scientific literature via
 109 LLMs, the framework effectively bridges data-rich and
 110 data-sparse regions in materials exploration. Our frame-



1 work demonstrates superior performance compared to
 2 traditional data-driven approaches and empirical phase
 3 selection rules, while achieving accuracy comparable to
 4 computationally expensive methods, particularly when
 5 predicting phase stability for compositions containing
 6 previously unseen elements. These results highlight that
 7 the significance of the framework does not reside in su-
 8 perseding established methods, but rather in effectively
 9 synthesizing their complementary strengths while repre-
 10 senting epistemic limitations transparently.

11 Beyond HEAs, this framework could accelerate dis-
 12 covery in several materials classes facing similar chal-
 13 lenges of vast compositional spaces and sparse data, in-
 14 cluding functional ceramics⁴⁴, and catalytic materials³⁴.
 15 Through successful validation on diverse alloy systems,
 16 this study demonstrates that uncertainty-aware AI in-
 17 tegration provides a viable path forward for accelerated
 18 materials discovery. The element substitutability pat-
 19 terns extracted using this framework may also inform
 20 synthetic strategies for targeted property optimization
 21 across diverse material applications.

22 AUTHOR CONTRIBUTIONS

23 M.-Q. H.: Conceptualization, Methodology, Software,
 24 Formal analysis, Validation, Investigation, Writing -
 25 Original Draft, Writing - Review & Editing, Visualiza-
 26 tion. D.-K. L.: Software, Investigation, Data Curation.
 27 V.-C. N.: Software, Formal analysis, Data Curation. H.
 28 K.: Investigation, Validation, Writing - Review & Edi-
 29 ting. S. C.: Investigation, Validation, Writing - Review &
 30 Editing. H.-C. D.: Conceptualization, Methodology, Val-
 31 idation, Investigation, Writing - Original Draft, Writing
 32 - Review & Editing, Visualization, Supervision, Project
 33 administration, Funding acquisition.

34 CONFLICT OF INTERESTS

35 The authors report there are no competing interests to
 36 declare.

37 DATA AVAILABILITY

38 **Publicly Available Datasets:** Data for this article,
 39 including experimental and computational datasets sup-
 40 porting high-entropy alloy phase prediction, are avail-
 41 able at Zenodo at <https://doi.org/10.5281/zenodo.17074832>.

43 **Code Availability:** Code for the uncertainty-
 44 aware AI integration framework is available at
 45 GitHub at <https://github.com/minhquyet2308/Uncertainty-Aware-AI-Integration>, with
 46 an archived version available at Zenodo at
 47 <https://doi.org/10.5281/zenodo.17744151>.

49 ACKNOWLEDGEMENTS

50 This work is supported by the JST-CREST Program
 51 (Innovative Measurement and Analysis), under Grant
 52 number JPMJCR2235; and the JSPS KAKENHI Grant
 53 Numbers 20K05301, JP19H05815, 20K05068, 23KJ1035,
 54 23K03950, and JP23H05403. S.C. acknowledges sup-
 55 port by US-DoD (ONR MURI program N00014-21-1-
 56 251). H. K. acknowledges support by the Japan Sci-
 57 ence and Technology Agency (JST) ASPIRE Program
 58 under the project "International Collaborative Research
 59 Network for Advanced Atomic Layer Processes". The
 60 authors thank Dr. Huan Tran and Dr. Xiomara Campi-
 61 longo for fruitful discussions.

62 REFERENCES

- 63 ¹J.-W. Yeh, S.-K. Chen, S.-J. Lin, J.-Y. Gan, T.-S. Chin, T.-
 64 T. Shun, C.-H. Tsau, and S.-Y. Chang, Advanced Engineering
 65 Materials **6**, 299 (2004).
- 66 ²B. Cantor, I. Chang, P. Knight, and A. Vincent, Materials Sci-
 67 ence and Engineering: A **375-377**, 213 (2004).
- 68 ³O. Senkov and D. Miracle, Journal of Alloys and Compounds
 69 **658** (2015), 10.1016/j.jallcom.2015.10.279.
- 70 ⁴J. M. Rickman, H. M. Chan, M. P. Harmer, J. A. Smeltzer, C. J.
 71 Marvel, A. Roy, and G. Balasubramanian, Nature Communica-
 72 tions **10**, 2618 (2019).
- 73 ⁵M.-H. Tsai and J.-W. Yeh, Materials Research Letters **2**, 107
 74 (2014).
- 75 ⁶C. Toher, C. Oses, D. Hicks, and S. Curtarolo, npj Comput.
 76 Mater. **5**, 69 (2019).
- 77 ⁷G. Deshmukh, N. J. Wichrowski, N. Evangelou, P. G. Ghanekar,
 78 S. Deshpande, I. G. Kevrekidis, and J. Greeley, npj Computa-
 79 tional Materials **10**, 116 (2024).
- 80 ⁸M. Ghorbani, M. Boley, P. N. H. Nakashima, and N. Birbilis,
 81 Scientific Reports **14**, 8299 (2024).
- 82 ⁹M.-H. Tsai, Entropy **18**, 252 (2016).
- 83 ¹⁰M.-H. Tsai, R.-C. Tsai, T. Chang, and W.-F. Huang, Metals **9**,
 84 247 (2019).
- 85 ¹¹W. Huang, P. Martin, and H. L. Zhuang, Acta Mater. **169**, 225
 86 (2019).
- 87 ¹²Z. Rao, P.-Y. Tung, R. Xie, Y. Wei, H. Zhang, A. Ferrari,
 88 T. Klaver, F. Körmann, P. T. Sukumar, A. K. da Silva, Y. Chen,
 89 Z. Li, D. Ponge, J. Neugebauer, O. Gutfleisch, S. Bauer, and
 90 D. Raabe, Science **378**, 78 (2022).
- 91 ¹³J. Roberts, B. Rijal, S. Divilov, J.-P. Maria, W. G. Fahrenholtz,
 92 D. E. Wolfe, D. W. Brenner, S. Curtarolo, and E. Zurek, npj
 93 Computational Materials **10**, 142 (2024).
- 94 ¹⁴D. Alman, Entropy **15**, 4504 (2013).
- 95 ¹⁵F. Zhang, C. Zhang, S. Chen, J. Zhu, W. Cao, and U. Kattner,
 96 Calphad **45**, 1 (2014).
- 97 ¹⁶M. Esters, C. Oses, S. Divilov, H. Eckert, R. Friedrich, D. Hicks,
 98 M. J. Mehl, F. Rose, A. Smolyanyuk, A. Calzolari, X. Campi-
 99 longo, C. Toher, and S. Curtarolo, Comp. Mat. Sci. **216**, 111808
 100 (2023).
- 101 ¹⁷C. Oses, M. Esters, D. Hicks, S. Divilov, H. Eckert, R. Friedrich,
 102 M. J. Mehl, A. Smolyanyuk, X. Campilongo, A. van de Walle,
 103 J. Schroers, A. G. Kusne, I. Takeuchi, E. Zurek, M. Buongiorno
 104 Nardelli, M. Fornari, Y. Lederer, O. Levy, C. Toher, and S. Curtarolo,
 105 Comp. Mat. Sci. **217**, 111889 (2023).
- 106 ¹⁸C. Toher and S. Curtarolo, Journal of Phase Equilibria and Dif-
 107 fusion **45**, 219 (2024).
- 108 ¹⁹Y. Lederer, C. Toher, K. S. Vecchio, and S. Curtarolo, Acta
 109 Materialia **159**, 364 (2018).



¹ ²⁰V. Stanev, C. Oses, A. G. Kusne, E. Rodriguez, J. Paglione, S. Curtarolo, and I. Takeuchi, *npj Comput. Mater.* **4**, 29 (2018).

² ²¹G. L. W. Hart, T. Mueller, C. Toher, and S. Curtarolo, *Nature Reviews Materials* **6**, 730 (2021).

³ ²²M.-Q. Ha, D.-N. Nguyen, V.-C. Nguyen, T. Nagata, T. Chikyow, H. Kino, T. Miyake, T. Denœux, V.-N. Huynh, and H.-C. Dam, *Nature Computational Science* **1**, 470 (2021).

⁴ ²³J. He, R. Yin, C. Wang, C. Liu, D. Xue, Y. Su, L. Qiao, T. Lookman, and Y. Bai, *Journal of Materiomics* **11**, 100913 (2025).

⁵ ²⁴T. L. Pham, H. Kino, K. Terakura, T. Miyake, K. Tsuda, I. Takigawa, and H. C. Dam, *Science and Technology of Advanced Materials* **18**, 756 (2017), pMID: 29152012.

⁶ ²⁵E. Hüllermeier and W. Waegeman, *Machine Learning* **110**, 457 (2021).

⁷ ²⁶E. Brochu, V. M. Cora, and N. de Freitas, “A tutorial on bayesian optimization of expensive cost functions, with application to active user modeling and hierarchical reinforcement learning,” (2010), arXiv:1012.2599 [cs.LG].

⁸ ²⁷J. Snoek, H. Larochelle, and R. P. Adams, in *Advances in Neural Information Processing Systems*, Vol. 25, edited by F. Pereira, C. Burges, L. Bottou, and K. Weinberger (Curran Associates, Inc., 2012).

⁹ ²⁸E. Hüllermeier and K. Brinker, *Fuzzy Sets and Systems* **159**, 2337 (2008), theme: Information Processing.

¹⁰ ²⁹E. P. George, D. Raabe, and R. O. Ritchie, *Nat. Rev. Mater.* **4**, 515 (2019).

¹¹ ³⁰T. Konno, H. Kurokawa, F. Nabeshima, Y. Sakishita, R. Ogawa, I. Hosako, and A. Maeda, *Phys. Rev. B* **103**, 014509 (2021).

¹² ³¹A. P. Dempster, *Journal of the Royal Statistical Society: Series B (Methodological)* **30**, 205 (1968).

¹³ ³²G. Shafer, *A Mathematical Theory of Evidence* (Princeton University Press, 1976).

¹⁴ ³³T. Denœux, D. Dubois, and H. Prade, in *A Guided Tour of Artificial Intelligence Research*, Vol. 1, edited by P. Marquis, O. Papini, and H. Prade (Springer Verlag, 2020) Chap. 4, pp. 119–150.

¹⁵ ³⁴N. Nu Thanh Ton, M.-Q. Ha, T. Ikenaga, A. Thakur, H.-C. Dam, and T. Taniike, *2D Materials* **8**, 015019 (2020).

¹⁶ ³⁵M.-Q. Ha, D.-N. Nguyen, V.-C. Nguyen, H. Kino, Y. Ando, T. Miyake, T. Denœux, V.-N. Huynh, and H.-C. Dam, *Journal of Applied Physics* **133**, 053904 (2023).

¹⁷ ³⁶E. O. Pyzer-Knapp, J. W. Pitera, P. W. J. Staar, S. Takeda, T. Laino, D. P. Sanders, J. Sexton, J. R. Smith, and A. Curioni, *npj Computational Materials* **8**, 84 (2022).

¹⁸ ³⁷D. H. Cook, P. Kumar, M. I. Payne, C. H. Belcher, P. Borges, W. Wang, F. Walsh, Z. Li, A. Devaraj, M. Zhang, M. Asta, A. M. Minor, E. J. Lavernia, D. Apelian, and R. O. Ritchie, *Science* **384**, 178 (2024).

¹⁹ ³⁸S. Liu, T. Wen, A. S. Pattamatta, and D. J. Srolovitz, *Materials Today* **80**, 240 (2024).

²⁰ ³⁹Z. Chen, Y. Liu, and H. Sun, *Nature Communications* **12**, 6136 (2021).

²¹ ⁴⁰B. Cantor, K. Kim, and P. J. Warren, in *Metastable, Mechanically Alloyed and Nanocrystalline Materials* (2001), *Journal of Metastable and Nanocrystalline Materials*, Vol. 13 (Trans Tech Publications Ltd, 2002) pp. 27–32.

²² ⁴¹D. Miracle and O. Senkov, *Acta Materialia* **122**, 448 (2017).

²³ ⁴²A. Tversky, *Psychological Review* **84**, 327 (1977).

²⁴ ⁴³P. Smets, *International Journal of Approximate Reasoning* **9**, 1 (1993).

²⁵ ⁴⁴S. Divilov, H. Eckert, D. Hicks, C. Oses, C. Toher, R. Friedrich, M. Esters, M. J. Mehl, A. C. Zettel, Y. Lederer, E. Zurek, J.-P. Maria, D. W. Brenner, X. Campilongo, S. Filipović, W. G. Fahrengoltz, C. J. Ryan, C. M. DeSalle, R. J. Crealese, D. E. Wolfe, A. Calzolari, and S. Curtarolo, *Nature* **625**, 66 (2024).

²⁶ ⁴⁵W. Chen, A. Hilhorst, G. Bokas, S. Gorsse, P. J. Jacques, and G. Hautier, *Nature Communications* **14**, 2856 (2023).

²⁷ ⁴⁶A. Takeuchi and A. Inoue, *MATERIALS TRANSACTIONS* **46**, 2817 (2005).

²⁸ ⁴⁷A. Takeuchi and A. Inoue, *Intermetallics* **18**, 1779 (2010).

²⁹ ⁴⁸T. Fukushima, H. Akai, T. Chikyow, and H. Kino, *Phys. Rev. Materials* **6**, 023802 (2022).

³⁰ ⁴⁹C. K. H. Borg, C. Frey, J. Moh, T. M. Pollock, S. Gorsse, D. B. Miracle, O. N. Senkov, B. Meredig, and J. E. Saal, *Scientific Data* **7**, 430 (2020).

³¹ ⁵⁰G. Khanna R, M. K. Singh, D. K. Rai, and S. Samal, *Materials Letters* **365**, 136404 (2024).

³² ⁵¹M. P. LaValley, *Circulation* **117**, 2395 (2008).

³³ ⁵²A. Seko, A. Togo, and I. Tanaka, “Descriptors for machine learning of materials data,” in *Nanoinformatics* (Springer Singapore, Singapore, 2018) pp. 3–23.

³⁴ ⁵³A. Seko, H. Hayashi, K. Nakayama, A. Takahashi, and I. Tanaka, *Phys. Rev. B* **95**, 144110 (2017).

³⁵ ⁵⁴F. C. T., *Nature* **138**, 7 (1936).

³⁶ ⁵⁵U. Mizutani, *MRS Bulletin* **37**, 169 (2012).

³⁷ ⁵⁶H. O. M. S. E. Mueller, in *Alloy Phase Diagrams* (ASM International, 2016).

³⁸ ⁵⁷Z. Pei, J. Yin, P. K. Liaw, and D. Raabe, *Nature Communications* **14**, 54 (2023).

³⁹ ⁵⁸X. Yang and Y. Zhang, *Materials Chemistry and Physics* **132**, 233 (2012).

⁴⁰ ⁵⁹S. Guo, Q. Hu, C. Ng, and C. Liu, *Intermetallics* **41**, 96 (2013).

⁴¹ ⁶⁰W. Zhijun, Y. Huang, Y. Yang, J. Wang, and C. Liu, *Scripta Materialia* **94** (2015), 10.1016/j.scriptamat.2014.09.010.

⁴² ⁶¹A. K. Singh, N. Kumar, A. Dwivedi, and A. Subramaniam, *Intermetallics* **53**, 112 (2014).

⁴³ ⁶²M. C. Troparevsky, J. R. Morris, P. R. C. Kent, A. R. Lupini, and G. M. Stocks, *Phys. Rev. X* **5**, 011041 (2015).

⁴⁴ ⁶³S. Guo, C. Ng, J. Lu, and C. T. Liu, *Journal of Applied Physics* **109**, 103505 (2011).

⁴⁵ ⁶⁴O. Senkov, G. Wilks, D. Miracle, C. Chuang, and P. Liaw, *Intermetallics* **18**, 1758 (2010).

⁴⁶ ⁶⁵B. S. Murty, J.-W. Yeh, S. Ranganathan, and P. P. Bhattacharjee, *High-Entropy Alloys*, 2nd ed. (Elsevier, Amsterdam, 2019).

⁴⁷ ⁶⁶J. Gild, Y. Zhang, T. Harrington, S. Jiang, T. Hu, M. C. Quinn, W. M. Mellor, N. Zhou, K. Vecchio, and J. Luo, *Scientific Reports* **6**, 37946 (2016).

⁴⁸ ⁶⁷S. Nakanowatari, K. Takahashi, H. C. Dam, and T. Taniike, *ACS Catalysis* **15**, 8691 (2025).

Data Availability Statement (DAS)

Publicly Available Datasets: Data for this article, including experimental and computational datasets supporting high-entropy alloy phase prediction, are available at Zenodo at <https://doi.org/10.5281/zenodo.17074832>.

Code Availability: Code for the uncertainty-aware AI integration framework is available at GitHub at <https://github.com/minhquyet2308/Uncertainty-Aware-AI-Intergration>, with an archived version available at Zenodo at <https://doi.org/10.5281/zenodo.17744151>.